

The Observed Offset Distribution of Gamma-Ray Bursts from Their Host Galaxies: A Robust Clue to the Nature of the Progenitors^{1,2}

Joshua S. Bloom, Shrinivas R. Kulkarni, S. George Djorgovski

Palomar Observatory 105–24, California Institute of Technology, Pasadena, CA 91125, USA

ABSTRACT

We present a comprehensive study to measure the location of γ -ray bursts (GRBs) relative to their host galaxies. In total, we find the offsets of 20 long-duration GRBs from their apparent host galaxy centers utilizing ground-based images from Palomar and Keck and public GRB datasets from the Hubble Space Telescope (HST). We discuss in detail how a host galaxy is assigned to an individual GRB and the robustness of the assignation process. The median projected angular (physical) offset is 0.36 arcsec (3.1 kpc). The median offset normalized by the individual host half-light radii is 1.2. We compare the observed offset distribution with the predicted burst locations of leading progenitor models. In particular, we compare the observed offset distribution with an exponential disk, a simplistic model for the location of collapsars and promptly bursting binaries (i.e., double helium star and black hole–white dwarf binaries). The statistical comparison shows remarkable agreement, with the Kolmogorov-Smirnov probability that the observed offsets derive from the model distribution of $P_{KS} = 0.52$. The case for a collapsar/promptly bursting binary origin is further strengthened with our observation that, in cases where there exists a preferred axis of the host galaxy, *every* GRB location is consistent with the semi-major axis. We also compare the observed GRB offsets with the expected offset distribution of delayed merging remnant progenitors (i.e., black hole–neutron star and neutron star–neutron star binaries). We find that delayed merging remnants progenitors, insofar as the predicted offset distributions are accurate, can be ruled out at better than the 10^{-3} level. This is arguably the strongest constraint yet against delayed merging remnants as the progenitors of long-duration GRBs. In the course of this study, we have also discovered the probable host galaxy of GRB 990510 in archival HST data.

¹Partially based on observations with the NASA/ESA Hubble Space Telescope, obtained at the Space Telescope Science Institute, which is operated by the Association of Universities for Research in Astronomy, Inc. under NASA contract No. NAS5-26555.

²In addition, some of the data presented herein were obtained at the W. M. Keck Observatory, which is operated as a scientific partnership among the California Institute of Technology, the University of California and the National Aeronautics and Space Administration, and was made possible by the generous financial support of the W. M. Keck Foundation.

Subject headings: astrometry—cosmology: miscellaneous — cosmology: observations — gamma rays: bursts—methods: statistical

1. Introduction

For some thirty years since the discovery of gamma-ray bursts (GRBs; Klebesadel et al. 1973), a basic understanding of the nature of the brief intense flashes of γ -rays remained elusive. Throughout much of the 1970s and 1980s the prevailing view was that GRBs arose from the surface of neutron stars in and around our Galaxy (see Lamb 1995, for a review), though, by the mid-1990s, the isotropic distribution of GRBs on the sky (cf. Fishman & Meegan 1995) served as the cornerstone of mounting evidence suggesting an extragalactic origin (see Paczyński 1995, for a review). The main impedance to progress was the difficulty of localizing bursts to an accuracy high enough to unequivocally associate an individual GRB with some other astrophysical entity. In large measure the localization problem was due to both the transient nature of the phenomena and the fact that the incident direction of γ -rays are difficult to pinpoint with a single detector; the typical $1-\sigma$ uncertainty in the location of a GRB using the *Burst and Transient Source Experiment* (BATSE) was 4–8 degree in radius (Briggs et al. 1999). The Interplanetary Network (IPN; cf. Cline et al. 1999) localized GRBs using burst arrival times at several spacecrafts throughout the Solar System and provided accurate localizations (\sim several arcmin in radius) to ground-based observers; however, the localizations were reported with large time delays (days to months after the GRB).

The crucial breakthrough came in early 1997, shortly following the launch of the BeppoSAX satellite (Boella et al. 1997). On-board instruments (Frontera et al. 1997; Jager et al. 1997) were used to rapidly localize the prompt and long-lived hard X-ray emission of the GRB of 28 February 1997 (GRB 970228) to an accuracy of 3 arcmin (radius) and relay the location to ground-based observers in a matter of hours. Fading X-ray (Costa et al. 1997) and optical (van Paradijs et al. 1997) emission, the so-called “afterglow,” associated with GRB 970228 were discovered. Ground-Based observers noted (Metzger et al. 1997b; van Paradijs et al. 1997) a faint nebulosity in the vicinity of the optical transient (OT) afterglow. Subsequent *Hubble Space Telescope* (HST) imaging resolved the nebulosity (Sahu et al. 1997) and showed that the morphology was indicative of a distant galaxy (Sahu et al. 1997). Three years later, we now know the redshift of this galaxy is $z = 0.695$ (Bloom et al. 2001). The next prompt localization of a GRB yielded the first confirmed distance to the GRB through optical absorption spectroscopy: GRB 970508 occurred from a redshift $z \geq 0.835$ (Metzger et al. 1997a). The first radio afterglow was detected from GRB 970508 which, through observations of scintillations, led to the robust inference of superluminal motion of the GRB ejecta (Frail et al. 1997). These measurements (along with the dozen other redshifts now associated with individual GRBs) have effectively ended the distance scale debate and solidified GRBs as one of the most extremely energetic phenomena known (cf. Kulkarni et al. 2000).

The cosmological nature of GRBs now frames our basic understanding of the physics of GRB phenomena³. The general energetics are well-constrained: given the observed fluences and redshifts, approximately 10^{52} erg in γ -ray radiation is released in a matter of a few seconds in every GRB. The GRB variability timescale suggests that that this energy is quickly deposited by a “central engine” in a small volume of space (radius of ~ 100 km) and is essentially optically thick to γ -ray radiation at early times. This opaque fireball of energy then expands adiabatically and relativistically until the γ -ray radiation can escape; the emitting surface of the GRB is likely to be 10^{15} – 10^{17} cm from the explosion site and probably arises from the interaction of internal shocks initiated by the central engine (e.g., Fenimore et al. 1999). Only a small amount of baryonic matter ($\sim 10^{-5} M_\odot$) can be entrained with the fireball since too much baryonic matter, a condition referred to as the “baryonic loading” problem, would essentially stall the relativistic expansion of the fireball. The transient afterglow phenomena is thought to be due to synchrotron radiation arising from the interaction of the relativistic ejecta and the ambient medium surrounding the burst site (see van Paradijs et al. 2000; Kulkarni et al. 2000, for reviews). The relativistic nature of the expanding shock (which also gives rise to the GRB) is required to avoid the so-called compactness problem (cf. Piran 1999) and, as mentioned above, was observational confirmed with radio scintillation measures of the afterglow of GRB 970508 (Frail et al. 1997).

While the observational phenomena is now reasonably well-understood, one large outstanding question remains: what makes a γ -ray burst? Specifically what are the astrophysical objects, the “progenitors”, which produce γ -ray bursts? The observations provide several clues which all appear to implicate the progenitors as stellar-mass systems involving a compact source, probably a black hole. First, the implied (isotropic) energy release in γ -rays are typically 10^{-3} – 10^{-1} times the restmass energy of the Sun. Further, the efficiency of conversion of the initial input energy (either Poynting flux or baryonic matter) to γ -rays is on the order of 1% (see Kumar 1999, and references therein); therefore, the best-guess estimate of the total energy release is roughly comparable to the restmass energy of one solar mass. Second, the variability timescale (few ms) observed implies the energy deposition takes place in a small region of space (radius of $c \times 1$ ms ≈ 30 km). Third, the inferred rate of GRB occurrence, about 4 per day in the Universe above current detection thresholds, and the lack of burst repetition (e.g., Hakkila et al. 1998) suggest that GRB events are rare ($\sim 10^{-7}$ yr $^{-1}$ Galaxy $^{-1}$; Fenimore et al. 1993; Wijers et al. 1998) and catastrophically destroy the individual progenitors. Fourth, the observed GRBs rate appears to be roughly proportional to the star-formation rate in the Universe.

The progenitor models which most naturally explain these observables in the GRB phenomena fall in to two broad classes—the coalescence of binary compact stellar remnants and the explosion of a massive star (“collapsar”). An active galactic nucleus (AGN) origin is another possibility, however the variability timescale still requires the energy source to be stellar-mass objects (Carter

³The emergent picture described herein is reserved to the so-called long duration GRBs, those lasting for a duration $\gtrsim 2$ sec, since no short-duration bursts have been well-localized on rapid timescales (\lesssim few days).

1992; Cheng & Wang 1999). In the following we briefly summarize the two popular classes and refer the reader to Fryer et al. (1999) for a more in-depth review. In both the collapsar and the merging remnant class of progenitors a spinning black hole is formed. The debris, either from the stellar core of the collapsar or a tidally disrupted neutron star, forms a temporary accretion disk (or “torus”) which then accretes into the black hole on a long timescale (~ 10 sec). In this general picture (see Rees 1999, for a review), the lifetime of the accretion disk accounts for the duration of the GRB and the light-crossing time of the black hole accounts for the variability timescale. The GRB is powered by the energy extracted either from the spin energy of the hole or the from the gravitational energy of the infalling matter.

The coalescing compact binary class (Paczyński 1986; Goodman 1986; Eichler et al. 1989) was favored before the first redshift determination because the existence of coalescence events of a double neutron star binaries (NS–NS) was assured; at least a few NS–NS systems in our Galaxy (e.g., PSR 1913+16, PSR 1534+12) will merge in a Hubble time thanks to the gravitational radiation of the binary orbital angular momentum (cf. Taylor 1994). Further, the best-estimate of the rate of NS–NS coalescence in the Universe (e.g., Phinney 1991; Narayan et al. 1992) was comparable to an estimate of the GRB rate (Fenimore et al. 1993; Wijers et al. 1998). Recently, stellar evolution models have suggested that black hole–neutron star binaries (BH–NS) may be formed at comparable rates to NS–NS binaries (e.g., Bethe & Brown 1998), though no such systems have been observed to-date. There are other merging remnant binaries in this class, notably merging black hole–white dwarf (BH–WD) binaries (Fryer & Woosley 1998) and merging helium star binaries (He–He) (cf. Fryer et al. 1999).

The collapsar class is comprised of a rotating massive star (either isolated or in a binary system) whose iron core subsequently collapses directly to form a black hole (Woosley 1993). To avoid baryon loading the progenitor star should have lost most, if not all, its extended gas envelope of hydrogen by the time of collapse. The progenitors of collapsars—likely Wolf-Rayet stars—then are closely related to the progenitors of hydrogen-deficient supernova, namely type Ib/Ic supernovae (cf. MacFadyen & Woosley 1999).

How can these two classes of progenitors be distinguished? For massive stars, the energy release from the collapse of the core of the star, just as in supernovae, is sufficient to explode the star itself. This may result in a supernova-like explosion at the essentially the same time as a GRB. The first apparent evidence of such a supernova associated with a cosmological GRB came with the discovery of a delayed bright red bump in the afterglow light curve of GRB 980326 (Bloom et al. 1999). The authors interpreted the phenomena as due to the light-curve peak of a supernova at redshift $z \sim 1$. Later, Reichart (1999) and Galama et al. (2000) found similar such red bump in the afterglow of GRB 970228. Merging remnant progenitors models (e.g., BH–NS, NS–NS systems) have difficulty producing such features in a light curve on such long timescales and so the supernova interpretation, if true, would be one of the strongest direct clues that GRBs come from massive star explosions. However, the supernova story is by no means complete. For instance, evidence of a supernova signature in other GRBs has not been found (Hjorth et al. 2000). Further, even the “supernova”

observations themselves find plausible alternative explanations (such as dust echoes) that do not strictly require a massive star explosion (Esin & Blandford 2000; Reichart 2001; Waxman & Draine 2000). We note, however, that all other plausible explanations of the observed late-time bumps require high-density environments found most readily in star forming regions.

Chevalier & Li (2000) make the important observation that if a GRB comes from a massive star, then the explosion does not take place not in a constant density medium, but medium enriched by constant mass loss from the stellar winds. One would expect to see signatures of this wind-stratified medium in the afterglow (e.g., bright sub-millimeter emission at early times, increasing “cooling frequency” with time; see Kulkarni et al. 2000). However, afterglow observations have been inconclusive (Kulkarni et al. 2000) with no clear evidence for a single GRB in such a medium.

Recent work has begun to focus on the immediate environments of GRBs as a means towards divining the nature of the progenitors. This has come primarily from detections of line features in several GRB afterglows (e.g., 970508 and 970828 Piro et al. 1999; Yoshida et al. 1999). The most recent and the most convincing detection so far from observations of the afterglow of GRB 991216 (Piro et al. 2001). Individually, the observational significance of the line detections are marginal but on the whole there appears to be a good case for line (emission) features in the afterglow of some GRBs. If so, the inescapable conclusion is that there must exist dense matter in the vicinity of the explosion (e.g., Weth et al. 2000; Vietri et al. 1999; Lazzati et al. 2000).

There is little doubt that stellar-mass like systems (merging remnants or explosions of massive stars) are responsible for the production of long-duration GRBs. Now, the thrust of the field should focus on determining which objects are the progenitors. Above we have reviewed a variety of observations used to-date to help distinguish collapsars and remnant mergers as the progenitors of GRBs. While most evidence points indirectly towards collapsars, the results are inconclusive owing in large part to the difficulty and subtlety of the observations required. In this paper we will examine an observationally robust clue (in analogy to SNe; see below), the location of GRBs with respect to galaxies. In §2 we review the expectations of GRB locations from each progenitor model. Then in §§3–4 we discuss the instruments, techniques, and expected uncertainties involved in constructing a sample of GRB locations about their host galaxies. In §5 we comment on the data reductions specific to each GRB in our sample. The observed distribution is shown and discussed in §6 and then statistically compared with the expected offset distribution of leading progenitor models (§7). Last, in §8 we summarize and discuss our findings.

2. Location of GRBs as a Clue to their Origin

Before the detailed modeling of light curves were used to constrain the nature of supernovae progenitors, the location of supernovae in and around galaxies provided important clues to the nature of the progenitors (e.g., Reaves 1953; Johnson & MacLeod 1963). For instance, only Type Ia supernovae have been found in elliptical galaxies naturally leading to the idea that the progenitor

population can be quite old whereas the progenitors of Type II and Type Ibc are likely to be closely related to recent star formation (cf. van Dyk 1992, for review). Further, in late-type galaxies, Type Ibc and Type II supernovae appear to be systematically closer to HII star forming regions than Type Ia supernovae (e.g., Bartunov et al. 1994). This is taken as strong evidence of that the progenitors of Type Ibc and Type II SNe are massive stars.

Since the most massive stars explode soon ($\lesssim 10^7$ yr) after zero-age main sequence (ZAMS), we expect GRBs from collapsars to be observed in galaxies undergoing vigorous star formation (*i.e.*, late-type, irregular, and starburst galaxies). Merging neutron stars on the other hand require a median time to merge of $\sim 2\text{--}10 \times 10^8$ yr since ZAMS (e.g., Phinney 1991; Narayan et al. 1992; Portegies Zwart & Spreeuw 1996; Bloom et al. 1999b). The instantaneous rate of GRBs from binary mergers, then, is more a function of the integrated (as opposed to instantaneous) star formation rate in its parent galaxy. So if GRBs arise from the death of massive stars we do not expect early-type (*i.e.*, elliptical and S0) host galaxies, whereas GRBs from merging remnants could occur in such galaxies. Further, due to the significant differences in time between ZAMS and mergers of NS–NS and BH–NS binaries, such merging remnants will produce GRBs at preferentially *lower* redshift than collapsars and promptly bursting binaries (He–He and BH–WD binaries).

More importantly, independent of galaxy type, the locations of GRBs within (or outside) of galaxies provide a powerful clue towards distinguishing the progenitor scenarios. Massive stellar explosions occur very near their birth-site, likely in active HII star-forming regions, since the time since ZAMS is so small. BH–WD binaries and He–He binaries will merge quickly and so are also expected to be located near star-forming regions (Fryer et al. 1999). In stark contrast, NS–NS and NS–BH binaries merge far from their birthsite. These stellar remnant progenitors will merge after at least one of the binary members has undergone a supernova. Each supernova is thought to impart a substantial “kick” on the resulting neutron star (cf. Hansen & Phinney 1997); for those binary systems which survive both supernovae explosions, the center-of-mass of the remnant binary itself will receive a velocity boost on the order of a few hundred km/s (e.g., Brandt & Podsiadlowski 1995). That is, NS–NS or NS–BH binaries will be ejected from their birthsite. The gradual angular momentum loss in the binary due to gravitational radiation causes the binary to coalescence (or “merge”) which then leads to a GRB. The exact time until merger ($\sim 10^6\text{--}10^9$ yr) depends on the masses of the remnants and binary orbit parameters. Population synthesis models have all shown $\sim 50\%$ of NS–NS and BH–NS binary mergers will occur beyond 10 kpc from centers of their host (Bloom et al. 1999b; Fryer et al. 1999).

How have locations within (or outside) of galaxies of GRB impacted our understanding of the progenitors of GRBs thus far? As mentioned above, the first accurate localization (van Paradijs et al. 1997) of a GRB by way of an optical transient afterglow revealed GRB 970228 to be spatially coincident with a faint galaxy (Sahu et al. 1997; Bloom et al. 2001). Though the coincident galaxy was faint, the *a posteriori* probability of a random location on the sky falling so close to a galaxy by chance was found to be low ($\sim 10\%$; van Paradijs et al. 1997). As such the galaxy was identified as the host of GRB 970228. Sahu et al. (1997) further noted that the OT appeared offset from

the center of the galaxy thereby calling into question an active galactic nucleus (AGN) origin. Soon thereafter Bloom et al. (1998) found, and then Fruchter & Pian (1998) confirmed, that GRB 970508 was localized very near the center of a dwarf galaxy. Given that underluminous dwarf galaxies have a weaker gravitational potential with which to bind merging remnant binaries, both Paczyński (1998) and Bloom et al. (1998) noted that the excellent spatial coincidence of the GRB with its putative host found an easier explanation with a massive star progenitor.

Unfortunately, the current instrumentation used for GRB observations cannot pinpoint or resolve individual GRB environments on the scale of tens of parsecs unless the GRB occurs a low redshift ($z \gtrsim 0.2$) and the transient afterglow is well-localized. Therefore the locations of most individual GRBs do not yield much insight into the nature of the progenitors. Instead, in this paper, we find the location (“offset”) of GRBs relative to the centers of their host galaxies and compare, analogous to SNe location comparisons with HII regions, the observed *distribution* with that expected from the of progenitor models. As we will demonstrate, though not all GRBs are well-localized, the overall distribution of GRB offsets proves to be a robust clue to the nature of the progenitors.

Several of the GRBs offset measurements have been determined previously by our group and others but we have reanalyzed every dataset currently available (with the exception of GRB 990712; see below). There are no major differences between older results and the offsets presented herein, but the offsets presented in this paper should be viewed as the current best results from our group. Throughout this paper we assume a flat Λ -cosmology (e.g., de Bernardis et al. 2000) with $H_0 = 65$ $\text{km s}^{-1} \text{Mpc}^{-1}$, $\Omega_M = 0.3$, and $\Lambda_0 = 0.7$.

3. The Data: Selection and Reduction

The primary goal of this paper is to measure the offsets of GRBs from their hosts where the necessary data are available. Ideally this could be accomplished using a homogeneous dataset of afterglow and host imaging. Though while HST is currently best suited for offsets studies given its exquisite angular resolution there are only a few early-time HST observations when the optical afterglow is still bright. On the other hand, ground-based observations of GRB afterglows are taken with different instruments, at different signal-to-noise levels, and through a variety observing conditions. Bearing these imperfections in mind we have compiled a dataset of images that we believe are best suited to find offsets of GRBs from their hosts.

A listing of the dataset compilation is given in Table 2. There is a hierarchy of preference of imaging conditions and instruments which yield the most accurate offsets; we describe the specifics and expected accuracies of the astrometric technique in §4.

3.1. Dataset selection based on expected astrometric accuracy

We group the datasets into 5 different levels ordered by decreasing astrometric accuracy. Levels 1–4 each utilized differential astrometry and level 5 utilizes absolute astrometry relative to the International Coordinate Reference System (ICRS). Specifics of the individual offset measurements are given in §4. The ideal dataset for offset determination is a single HST image where both the transient and host are well-localized (hereafter “self-HST”); so far, only GRB 970228 and GRB 990123 fall in to this category. The next most accurate offset is obtained where both the early- and late-time images are from HST taken at comparable depth with the same filter (hereafter “HST→HST”). In addition to the centering errors of the OT and host, such a set inherits the uncertainty in registering the two epochs (e.g., GRB 970508). Next, an early deep image from ground-based (GB) Keck, Palomar 200-inch (P200), or the Very Large Telescope (VLT) in which the OT dominates is paired with a late-time image from HST (e.g., GRB 971214, GRB 980703, GRB 991216, GRB 000418; “GB→HST”). Though in the majority of these cases most of the objects detected in the HST image are also detected in the Keck image (affording great redundancy in the astrometric mapping solution), object centering of ground-based data is hampered by atmospheric seeing. The next most accurate localization, use ground-based to ground-based imaging to compute offsets (“GB→GB”). Lastly, radio localizations compared with optical imaging (“VLA→GB”) provide the least accurate offset determinations. This is due primarily to the current difficulty of mapping an optical image onto an absolute coordinate system (see §4.0.7).

3.2. Imaging Reductions

3.2.1. Reductions of HST Imaging

The principal HST CCD imager used so far for GRB imaging is the *Space Telescope Imaging Spectrograph* (STIS; Kimble et al. 1998). However STIS imaging undersamples the angular diffraction limit of the telescope. Therefore, individual HST images essentially do not contain the full astrometric information possible. To produce a final image that is closer to the diffraction limit, interpixel dithering between multiple exposures is required. The image reconstruction technique, which also facilitates removal of cosmic-rays and corrects for known optical field distortion, is called “drizzling” and is described in detail in Fruchter & Hook (1997). We use this method, as implemented using the IRAF⁴ package DITHER and DITHERII.

We retrieved and reduced every public STIS dataset of GRB imaging from the HST archive⁵ and processed the so-called “On-the-Fly Calibration” images to produce a final drizzled image.

⁴IRAF is distributed by the National Optical Astronomy Observatories, which are operated by the Association of Universities for Research in Astronomy, Inc., under cooperative agreement with the National Science Foundation.

⁵<http://archive.stsci.edu>

These images are reduced through the standard HST pipeline for bias subtraction, flat-fielding, and illumination corrections using the best calibration data available at the time of archive retrieval. The archive name of the last image and the start time of each HST epoch are given columns (2) and (3) in Table 1.

Some HST GRB imaging has been taken using the STIS/Longpass filter (F28x50LP) which, based on its red effective wavelength (central wavelength $\lambda_c \approx 7100\text{\AA}$), would make for a good comparison with ground-based *R*-band imaging. However, the Longpass filter truncates the full STIS field of view to about 40% and therefore systematically contains fewer objects to tie astrometrically to ground-based images. Therefore, all of the HST imaging reported herein were taken in (unfiltered) STIS/Clear (CCD50) mode. Unlike the Longpass filter, the spectral response of the Clear mode is rather broad (2000–10000 \AA). We use the known optical distortion coefficients appropriate to the wavelength of peak sensitivity $\lambda \approx 5850 \text{ \AA}$ of this observing mode to produce final images which are essentially linear in angular displacement versus instrumental pixel location.

The original plate scale of most STIS imaging is $0''.05077 \text{ pixel}^{-1}$, though there is a possibility that thermal expansion of the instrument could change this scale by a small amount (see Appendix A). The pixel scale of all our final reduced HST images is half the original scale, *i.e.*, $0''.02539 \text{ pixel}^{-1}$.

3.2.2. *Reductions of Ground-Based Imaging*

Ground-Based images are all reduced using standard practice for bias subtraction, flat-fielding, and in the case of *I*-band imaging, fringe correction. In constructing a final image we compute the instrumental shift of dithered exposures relative to a fiducial exposure and coadd the exposures after applying the appropriate shift to align each image. All images are visually inspected for cosmic-ray contamination of the transient, host or astrometric tie stars. Pixels contaminated by cosmic rays are masked and not used in the production of the final image.

4. Astrometric Reductions and issues related to dataset levels

Here we provide a description of the astrometric reduction techniques for both our ground-based and the HST images and issues related to the five levels of astrometry summarized in §3.1. A discussion of the imaging reductions and astrometry for the individual cases is given in section §5.

4.0.3. *Level 1: “self-HST astrometry”*

An ideal image is one where the optical transient and the host galaxy are visible in the same imaging epoch with HST. This typically implies that the host galaxy is large enough in extent to be well-resolved despite the brilliance of the nearby OT. Of course, a later image of the host is always helpful to confirm that the putative afterglow point source does indeed fade. In this case (as with GRB 970228 and GRB 990123) the accuracy of offset determination is limited mostly by the centroiding errors of the host “center” and optical afterglow. Uncertainties in the optical distortion corrections and the resulting plate scale are typically sub-milliarcssecond in size (see Appendix A).

In principle we expect centering techniques to result in centroiding errors (σ_c) on a point source with a signal-to-noise, SN, of $\sigma_c \approx \phi/SN$ (cf. Stone 1989), where ϕ is the instrumental full-width half maximum (FWHM) seeing of the final image. Since ϕ is typically ~ 75 milliarcssecond (mas) we expect \sim milliarcssecond offset accuracies with self-HST images.

4.0.4. *Level 2: HST→HST*

Here, two separate HST epochs are used for the offset determination. The first epoch is taken when the afterglow dominates the light and the second when the host dominates. In addition to the centroiding errors, this level inherits the uncertainty of the registration of the two images.

In general when two images are involved (here and all subsequent levels), we need to register the two images such that an instrumental position in one image is mapped to the instrumental (or absolute position) in the other image. The registration process is as follows. We determine the noise characteristics of both of the initial and final images empirically, using an iterative sigma-clipping algorithm. This noise along with the gain and effective read noise of the CCD are used as input to the IRAF/CENTER algorithm. In addition we measure the radial profile of several apparent compact sources in the image and use the derived seeing FWHM (ϕ) as further input to the optimal filtering algorithm technique for centering (OFILTER; see Davis 1987). For faint stars we use the more stable GAUSSIAN algorithm. Both techniques assume a Gaussian form of the point-spread function which, while not strictly matched to the outer wings of the Keck or HST PSFs, appears to reasonably approximate the PSF out to the FWHM of the images.

When computing the differential astrometric mappings between two images (such as HST and Keck or Keck and the USNO-A2.0 catalogue) we use a list of objects common from both epochs, “tie objects”, and compute the astrometric mapping using the routine IRAF/GEOGRAPH. The polynomial order of the differential fitting we use depends on the number of tie objects. A minimum of 3 tie objects are required to find the relative rotation, shift and scale of two images, which leaves only one degree of freedom. The situation is never this bad: in fact, when comparing HST images and an earlier HST image (or deep Keck image) we typically find 20–30 reasonable tie objects and therefore we can solve for higher-order distortion terms. Figure 1 shows an example

Keck and HST field of GRB 981226 and the tie objects we use for the mapping. We always reject tie objects that deviate by more than 3σ from the initial mapping. A full third-order 2-dimensional polynomial with cross-terms requires 18 parameters which leaves, typically, $N \approx 30$ degrees of freedom. Assuming such a mapping adequately characterizes the relative distortion, it is reasonable to expect that mapping errors will have an r.m.s. error $\sigma \approx 30^{-1/2}\phi/\langle SN \rangle$, where $\langle SN \rangle$ is the average signal-to-noise of the tie objects. For example, in drizzled HST images $\phi \approx 75$ mas and $\langle SN \rangle \approx 20$ so that we can expect differential mapping uncertainties at the 1 mas level for HST→HST mapping. Cross-correlation techniques, such as IRAF/CROSSDRIZZLE, can in principle result in even better mapping uncertainties, but, in light of recent work by Anderson & King (1999), we are not confident that the HST CCD distortions can reliably removed at the sub-mas level.

4.0.5. Level 3: GB→HST

This level of astrometry accounts for the majority of our dataset. In addition to inheriting the uncertainties of centroiding errors and astrometric mapping errors described above, we must also consider the effects of differential chromatic refraction (DCR) and optical image distortion in ground based images. In Appendix A we demonstrate that these effects do not dominate the offset uncertainties. Following from the argument above (§4.0.4) the astrometric mapping accuracies scale linearly with the seeing of ground-based images, typically a factor of 10–20 larger than the effective seeing of the HST images.

An independent test of the accuracy of the transference of differential astrometry from ground-based images to spaced-based imaging is illustrated by the case of GRB 990123. In Bloom et al. (1999a) we registered a Palomar 60-inch (P60) image to a Keck image and thence to an HST image. The overall statistical uncertainty (see Appendix B for a derivation) of this was $\sigma_r = 107$ mas (note, that in the original paper we mistakenly overstated this error as 180 mas uncertainty). The position we inferred was 90 mas from a bright point source in the HST image. This source was later seen to fade in subsequent HST imaging and so our identification of the source as the afterglow from P60→Keck→HST astrometry was vindicated. Since the P60→Keck differential mapping accounted for the majority of the error (due to optical field distortion and unfavorable seeing in P60), we consider ~ 100 mas uncertainty in Keck→HST mapping as a reasonable upper limit to the expected uncertainty from other cases.

4.0.6. Level 4: GB→GB

This level contains the same error contributions as in GB→HST level, but in general, the uncertainties are larger since the centroiding uncertainties are large in both epochs. The offsets are computed in term of pixels in late-time image. Just as with the previous levels with HST, we

assume an average plate scale to convert the offset in to units of arcseconds. For LRIS (Oke et al. 1995) and ESI (Epps & Miller 1998) imaging we assume a plate scale of $0''.212 \text{ pixel}^{-1}$ and $0''.153 \text{ pixel}^{-1}$, respectively. We have tested that these plate scales are stable over time to better than 5%; that is, the errors introduced by any deviations from these assumed plate scales are negligible.

4.0.7. Level 5: VLA→GB or VLA→HST

Unfortunately, the accuracy of absolute offset determination is (currently) hampered by systematics in astrometrically mapping deep optical/infrared imaging to the ICRS. Only bright stars ($V \lesssim 9$ mag) have absolute localizations measured on the milliarcsecond level thanks to astrometric satellite missions such as Hipparcos. The density of Hipparcos stars is a few per square degree so the probability of having at least two such stars on a typical CCD frame is low. Instead, optical astrometric mapping to the ICRS currently utilizes ICRS positions of stars from the USNO-A2.0 Catalogue, determined from scanned photographic plates (Monet 1998). Even if all statistical errors of positions are suppressed, an astrometric plate solution can do no better than inherit a systematic $1-\sigma$ uncertainty of 250 mas in the absolute position of any object on the sky ($\sigma_\alpha = 0''.18$ and $\sigma_\delta = 0''.17$; Deutsch 1999). By contrast, very-long baseline array (VLBA) positions of GRB radio afterglow have achieved sub-milliarcsecond absolute positional uncertainties relative to the ICRS (Taylor et al. 1999). So until optical systematics are beaten down and/or sensitivities at radio wavelengths are greatly improved (so as to directly detect the host galaxy at radio wavelengths), the absolute offset astrometry can achieve $1-\sigma$ accuracies no better than ~ 300 mas (≈ 2.5 kpc at $z = 1$).

There are four GRBs in our sample where absolute astrometry (level 5) is employed. In computing the location of the optical transient relative to the ICRS we use typically 20–40 USNO A2.0 astrometric tie stars in common with Keck or Palomar images. We then use IRAF/CCMAP to compute the mapping of instrumental position (x,y) to the world coordinate system (α, δ).

5. Individual Offsets and Hosts

Below we highlight the specific reductions for each offset, the results of which are in Table 2. In our analysis which follows we do not include observations of GRB 990308 since it is unclear as to the true nature of the transient optical source observed on a single epoch (Schaefer et al. 1999). In all there are 23 bursts that have been reliably localized at the arcsecond level and 1 burst with an uncertain association with a nearby SN (GRB 980425). We do not include analysis on the recent bursts GRB 000210 (Stornelli et al. 2000), GRB 000630 (Hurley et al. 2000a), GRB 000911 (Hurley et al. 2000b), GRB 000926 (Hurley et al. 2000c) due to lack of imaging data of the hosts. Thereby, the present study includes 19 “cosmological” GRBs plus the nearby SN 1998bw/GRB 980425.

To look for the host of a GRB, in general, we image each GRB field roughly a few months to a

year after the burst with Keck (similarly at the VLT in the South). Typically these observations reach a limiting magnitude of $R \approx 24\text{--}26$ mag depending on the specifics of the observing conditions. If an object is detected within ~ 1 arcsec from the afterglow position and has a brightness significantly above the extrapolated afterglow flux at the time of observation, this source is deemed the host (most GRB hosts are readily identified in such imaging). If no object is detected, we endeavor to obtain significantly deeper images of the field. Typically these faint host searches require 1–3 hours of Keck (or VLT) imaging to reach limiting magnitudes at the $R \approx 27$ mag level. If no object is detected at the location of the afterglow, HST imaging is required and the host search is extended to limiting magnitudes of $R \approx 28\text{--}29$ mag. Only 1 host in our sample (GRB 990510; Bloom 2000 and this paper) has been first found using HST after an exhaustive search from the ground.

It is important to note that the assignment of a certain observed galaxy as the host of a GRB is, to some extent, a subjective process. This host center assignment is notably most subjective when the apparent host has several bright components (e.g., GRB 980613). Yet irrespective of the *validity* of individual assignments of hosts, we uniformly assign the nearest (in angular distance) detected galaxy as the host. The center of the assigned host is then, except in a few cases, determined as the centroid near the brightest component of the host system. Clearly the host detection magnitude limits vary from GRB to GRB, but recalling that our search technique would be exhaustive to $R \sim 28$ mag should no obvious hosts be found to shallower depths, the entire sample is unified by setting a very conservative detection limit for all GRB hosts at the $R \approx 28$ mag level. Therefore, in some statistical sense, *the offset distribution we find herein may be considered a distribution of GRB positions from the nearest respective detected galaxy with $R \lesssim 28$ mag*. This is clearly a conservative reduction of the host detection limits, but this reduction allows us in §6.1 to formulate a robust upper limit to the probability that GRBs are associated with galaxies by chance. In §6.1 we also discuss how absorption/emission redshifts help strengthen the physical connection of GRBs to their assigned hosts.

A summary of our offset results is presented in Table 2. Since all our final images of the host galaxies are rotated to the cardinal orientation before starting the astrometric mapping process, these uncertainties are also directly proportional to the uncertainties in α and δ . It is important to note, however, that the projected radial offset is a positive-definite number and the probability distribution is not Gaussian. Thereby, the associated error (σ_r) in offset measurements does not necessarily yield 68% confidence region for offset (see Appendix B) but is, clearly, indicative of the precision of the offset measurement.

5.1. GRB 970228

The morphology and offset derivation have been discussed extensively in Bloom et al. (2001) and we briefly summarize the results. In the HST/STIS image (Fig. 2), the host appears to be essentially a face-on late-type blue dwarf galaxy. At the center is an apparent nucleus manifested as a 6σ peak north of the transient. There is also an indication of arm-like structure extending

towards the transient.

This image represents the ideal for astrometric purposes (level 1): both the transient and the host “center” are well-localizable in the same high-resolution image. The transient appears outside the half-light radius of the galaxy.

5.2. GRB 970508

The host is a compact, elongated and blue (Bloom et al. 1998) and is likely undergoing a starburst phase. The optical transient was well-detected in the early time HST image (Pian et al. 1998) and the host was well-detected (Fig. 2) in the late-time image (Fruchter & Pian 1998). We masked out a $2'' \times 2''$ region around the OT/host and cross-correlated the two final images using the IRAF/CROSSDRIZZLE routine. We used the IRAF/SHIFTFIND routine on the correlation image to find the systematic shift between the two epochs. The resulting uncertainty in the shift was quite small, $\sigma = 0.013, 0.011$ pix (x,y direction). We also found 37 compact objects in common to both images and performed an astrometric mapping in the usual manner and find $\sigma = 0.344, 0.354$ pix in the (x,y directions). We centered the OT and the host in the normal manner using the IRAF/ELLIPSE task.

The resulting offset is given in Table 2 where we use the more conservative astrometric mapping uncertainties from using the tie objects, rather than the CROSSDRIZZLE routine. As first noted in Bloom et al. (1998) (Keck imaging) and then in Fruchter & Pian (1998) (HST imaging), the OT was remarkably close to the apparent center of the host galaxy. The P200→Keck astrometry from Bloom et al. (1998) produced an r.m.s. astrometric uncertainty of 121 mas, compared to an r.m.s. uncertainty of 11 mas from HST→HST astrometry. The largest source of uncertainty from the HST→HST is the centroid position of the host galaxy.

5.3. GRB 970828

The host is identified as the middle galaxy in an apparent 3-component system. We discuss the host properties and the astrometry (VLA→Keck) in more detail in Djorgovski et al. (2000). The total uncertainty in the radio to Keck tie is 506 mas (α) and 376 mas (δ).

5.4. GRB 971214

By all accounts, the host appears to be a typical L_* galaxy at redshift $z = 3.42$. The Keck→HST astrometry is discussed in detail in Odewahn et al. (1998). The offset uncertainty found was $\sigma_r = 70$ mas. The GRB appears located to the east of the host galaxy center, but consistent with the east-west extension of the host (see Figure 2).

5.5. GRB 980326

Bloom et al. (1999) reported that no host has been found at the position of the optical transient down to a 3σ limiting magnitude of $R \approx 27.3$ mag. In all likelihood, the host is simply fainter than this limiting magnitude. However, there are several faint galaxies detected in the vicinity of the optical transient. The nearest appears object to be an elongated galaxy with $R \sim 26.5$ mag which is at a distance of $2''.6 \pm 0''.2$ to the west of the GRB. In the interest of uniformity of all datasets, we tentatively assign this galaxy as the host, but we believe that this host assignment is probability incorrect (discussed below). Deep HST imaging has been planned to search for a more nearby host to a fainter magnitude limit than our Keck imaging.

5.6. GRB 980329

Despite the good radio localization of the afterglow (Taylor et al. 1998b) we only have a late-time optical image from Keck for comparison. We found an astrometric plate solution using 28 field stars in the USNO-A2.0 catalogue. The statistical uncertainties were 271 mas and 253 mas in α and δ , respectively. Including the radio positional uncertainty and the systematic uncertainty in the optical tie to the ICRS, the 1σ uncertainties in the radio position on our final optical image is 324 mas and 314 mas (α, δ).

As showing in Fig. 2, the GRB is coincident with a slightly extended faint galaxy. The angular offset (cf. Table 2) of the GRB from this galaxy is negligible to within the astrometric error.

5.7. GRB 980425

The SN 1998bw was well-localized at radio wavelengths (Wieringa et al. 1998) with an astrometric position relative to the ICRS of 100 mas in each coordinate. Ideally we could calibrate the HST/STIS image to ICRS to ascertain where the radio sources lies. However, without Hipparcos/Tycho astrometric sources or radio point sources in the STIS field such absolute astrometric positioning is difficult.

Instead, we registered an early ground-based image to the STIS field to determine the differential astrometry of the optical SN with respect to its host. Unfortunately most early images were relatively shallow exposures to avoid saturation of the then bright SN and so many of the point sources in the STIS field are undetected. The best seeing and deepest exposure from ground-based imaging is from the EMMI/ESO NTT 3.5 meter Telescope on 4.41 May 1998 (Galama 1999) where the seeing was 0.9 arcsec FWHM. We found 6 point sources which were detected in both the STIS/CLEAR and the ESO NTT I -band image. The use of I -band positions for image registration is justified since all 6 point sources are red in appearance and therefore unlikely to introduce a systematic error in the relative positioning. Since the number of astrometric tie sources is low, we

did not fit for high-order distortions in the ESO image and instead we fit for the relative scale in both the x and y directions, rotation, and shift (5 parameters for 12 data points). We compute an r.m.s. uncertainty of 40 mas and 32 mas in x and y positions of the astrometric tie sources. These transformation uncertainties dominate the error in the positional uncertainty of the SN in the ESO NTT image and so we take the transformation uncertainties as the uncertainty in the true position of the supernova with respect to the STIS host image.

The astrometric mapping places the optical position of SN 1998bw within an apparent star-forming region in the outer spiral arm of the host 2.4 kpc in projection at $z = 0.0088$ to the southwest of the galactic nucleus. Within the uncertainties of the astrometry the SN is positionally coincident with a bright, blue knot within this region, probably an HII region. This is consistent with the independent astrometric solutions reported in Fynbo et al. (2000b).

5.8. GRB 980519

The GRB afterglow was well-detected in our early-time image from the Palomar 200-inch. We found 150 objects in common to this image and our intermediate-time Keck image. An astrometric registration between the two epochs was performed using *IRAF/GEOMAP*. Based on this astrometry, Bloom et al. (1998) reported the OT to be astrometrically consistent with a faint galaxy, the putative host. This is the second faintest host galaxy (after GRB 990510; see below) observed to date with $R = 26.1 \pm 0.3$.

We found 25 objects in common with the intermediate-time Keck image and the HST/STIS image. These tie objects were used to further propagate the OT position onto the HST frame. Inspection of our final HST image near the optical transient location reveals the presence of low surface-brightness emission connecting the two bright elongated structures. Morphologically, the “host” appears to be tidally interacting galaxies, although this interpretation is subjective. The GRB location is coincident with the the dimmer elongated structure to the north. We estimated the center of the host, albeit somewhat arbitrarily, as the faint knot south of the GRB location and to the east of the brighter elongated structure. The half-light radius of the system was also measured from this point. From this “center” we find the offset of the GRB given in Table 2.

5.9. GRB 980613

The morphology of the system surrounding the GRB is complex and discussed in detail in Djorgovski et al. (2001). There we found the OT to be within ~ 3 arcsec of 5 apparent galaxies or galaxy fragments two of which are very red ($R - K > 5$). Including the centering errors and the registration uncertainty we find the OT was offset from the brightest R -band component by $0''.52 \pm 0''.13$ East and $0''.83 \pm 0''.14$ S. We interpret the brightest R -band component as host galaxy of the GRB.

5.10. GRB 980703

The optical transient was well-detected in our early time image and, based on the light curve and the late-time image, the light was not contaminated significantly with light from the host galaxy. We found 23 objects in common to the Keck image and our final reduced HST/STIS image and computed the geometric transformation. The r.m.s. uncertainty of the OT position on the HST image was quite small: 49 mas and 60 mas in the instrumental x and y coordinates, respectively. We determined the center of the host using *IRAF/ELLIPSE* and *IRAF/CENTER* which gave consistent answers to 2 mas in each coordinate.

5.11. GRB 981226

Unfortunately, no optical transient was found for this burst but a radio transient was identified (Frail et al. 1999). We rely on the transformation between the USNO-A2.0 and the Keck image to place the host galaxy position on the ICRS (see Frail et al. 1999, for further details). We then determined the location of the radio transient in the HST frame using 25 compact sources common to both the HST and Keck image. In Figure 1 we show as example the tie objects in both the Keck and HST image. The tie between the two images is excellent: 33 mas and 47 mas in the instrumental x and y positions (1σ). Clearly, the uncertainty in the radio position on the Keck image dominates the overall location of the GRB on the HST image.

The host appears to have a double nucleated morphology, perhaps indicative of a merger or interacting system. Hjorth et al. (2000) noted, by inspecting both the STIS Longpass and the STIS clear image, that the north-eastern part of the galaxy appeared significantly bluer than the south-western part. As expected from these colors the center of the host as measured in our late-time *R*-band Keck lies near (~ 50 mas) the centroid of the red (south-western) portion of the host. We assign the *R*-band centroid in Keck image as the center of the host.

5.12. GRB 990123

This GRB had an extremely bright prompt optical afterglow emission which was found archivally by a robotic telescope, the Robotic Optical Transient Search Experiment (ROTSE) (Akerlof et al. 1999). We reported on the astrometric comparison of ground-based data with HST imaging and found that the bright point source on the southern edge of a complex morphological system was the afterglow (Bloom et al. 1999a). Later HST imaging revealed that indeed this source did fade (e.g., Fruchter et al. 1999a) as expected of GRB afterglow.

As seen in Figure 2, the host galaxy is fairly complex, with two bright elongated regions spaced by $\sim 0''.5$ which run approximately parallel with each other. The appearance of spatially curved emission to the west may be a tidal tail from the merger of two separate systems or a pronounced

spiral arm of the brighter elongated region to the north. We chose, again somewhat subjectively, the peak of this brighter region as the center of the system and find the astrometric position of the GRB directly from the first HST epoch.

5.13. GRB 990506

The Keck astrometric comparison to the radio position was given in Taylor et al. (2000), with a statistical error of 250 mas. We transferred this astrometric tie to the HST/STIS image using 8 compact sources common to both the Keck and HST images of the field near GRB 990506. The resulting uncertainty is negligible compared to the uncertainties in the radio position on the Keck image. As first reported in Taylor et al. (2000), the GRB location appears consistent with a faint compact galaxy. Hjorth et al. (2000a) later reported that the galaxy appears compact even in the STIS imaging.

5.14. GRB 990510

This GRB is well-known for having exhibited the first clear evidence of a jet manifested as an achromatic break in the light curve (e.g., Harrison et al. 1999; Stanek et al. 1999). Recently, we discovered the host galaxy in late-time HST/STIS imaging (Bloom 1999) with $V = 28.5 \pm 0.5$. Registration of the early epoch where the OT was bright reveals the OT occurred 64 ± 9 mas west and 15 ± 12 mas north of the center of the host galaxy. This amounts to a significant displacement of 66 ± 9 mas or 600 pc at a distance of $z = 1.62$ (Galama et al. 1999). The galaxy is extended with a position angle $PA = 80.5 \pm 1.5$ degree (east of north) with an ellipticity of about ~ 0.5 . The host does appear to be marginally detected in the July 1999 imaging as well (although see, Fruchter et al. 1999b).

5.15. GRB 990705

Masetti et al. (2000) discovered the infrared afterglow of GRB 990705 projected on the outskirts of the Large Magellanic Cloud. At the position of the afterglow, Masetti et al. (2000) noted an extended galaxy seen in ground-based V -band imaging; they identified this galaxy as the host. Recently, Holland et al. (2000c) reported on HST imaging of the field and noted, thanks to the large size (~ 2 arcsec) of the galaxy and resolution afforded by HST, an apparent face-on spiral at location of the transient. We retrieved the public HST data and compared the early images provided by N. Masetti with our final reduced HST image. Consistent with the position derived by Holland et al. (2000c), we find that the transient was situated in a spiral arm to the west of the galaxy nucleus and just north of an apparent star-forming region.

The redshift of the host galaxy is not known. However, given the apparent angular size of the galaxy, it likely resides at $z \approx 0.15\text{--}0.35$. We masked out bright stars in the region around the host galaxy and found the half-light radius to be $R_{\text{half}} = 1.10 \pm 0.05$ arcsec. At a redshift of $z = 0.25$ this corresponds to $R_{\text{half}} = 4.6$ kpc, typical for a spiral galaxy.

5.16. GRB 990712

This GRB is the lowest measured redshift of a “cosmological” GRB with $z = 0.4337$ (Hjorth et al. 2000). Unfortunately, the astrometric location of the GRB appears to be in question, though there is no question that the GRB occurred within the bright galaxy pictured in Fig. 2. Hjorth et al. 2000 found that the only source consistent with a point source in the earlier HST image was the faint region to the Northwest side of the galaxy and concluded that the source was the optical transient. However, Fruchter et al. (2000) found that this source did not fade significantly. Instead the Fruchter et al. analysis showed, by subtraction of two HST epochs, that a source did fade near the bright region to the southeast. While the fading could be due to AGN activity instead of the presence of a GRB afterglow, we adopt the conclusion of Fruchter et al. for astrometry and place conservative uncertainties on the location relative to the center as 75 mas (3 pixels) in both α and δ for $1\text{-}\sigma$ errors. We did not conduct an independent analysis to determine this GRB offset.

5.17. GRB 991208

In our early K -band image of the field, we detect the afterglow as well as 5 suitable tie stars to our late ESI image. We computed only the relative shift, scale, and rotation of the two images. The resulting angular offset reported in Table 2 was first reported in Diercks et al. (2000). The host galaxy appears extended with an ellipticity of ~ 0.3 and $\text{PA} = 106 \pm 6$ degree.

5.18. GRB 991216

We used 9 compact objects in common to our early Keck image (seeing $\text{FWHM} = 0''.66$) and the late-time HST/STIS imaging to locate the transient. As noted first by Vreeswijk et al. (2000), the OT is spatially coincident with a faint, apparent point source in the HST/STIS image. Our astrometric accuracy of $\sigma_r = 32$ mas of the OT position is about 4 times better than that of Vreeswijk et al. (2000). Thanks to this we can confidently state that the OT coincides with a point source on the HST/STIS image. We believe this point source, as first suggested by Vreeswijk et al., is the OT itself.

The “location” of the host galaxy is difficult to determine. The OT does appear to reside to the southwest of faint extended emission (object “N” from Vreeswijk et al. 2000) but it is also

located to the northeast of a brighter extended component (object “S” from Vreeswijk et al. 2000). There appears to be a faint bridge of emission connecting the two regions as well as the much larger region to the west of the OT (see Fig. 2). In fact these three regions may together comprise a large, low-surface brightness system. Again, somewhat arbitrarily, we take the center of the “host” to be the peak of object “S”.

5.19. GRB 000301C

Fruchter et al. (2000a), in late-time imaging of the field of GRB 000301C, found no evidence for an underlying galaxy. They place a limit on the host brightness at $V \gtrsim 28.5$ mag. In Figure 2 we show the early-time image from HST/STIS. A galaxy $2''.13$ from the transient to the northwest is detected at $R = 24.25 \pm 0.08$ mag and shown in Figure 2. It is possible that this galaxy may be the host in which case the angular offset from the OT would amount to a projection of 19.2 kpc at redshift $z = 2.03$. However, given the bright apparent magnitude of this galaxy ($R = 24.25$) and the moderately high redshift ($z = 2.03$) of the GRB inferred from absorption spectroscopy (Smette et al. 2001; Castro et al. 2000), the galaxy is likely a foreground object (see also Garnavich et al. 2001). In this respect, both deeper HST imaging of the field after the transient fades and spectroscopy of the bright galaxy should help clear up the ambiguity.

5.20. GRB 000418

We reported the detection of an optically bright component and an infrared bright component at the location of GRB 000418 (Bloom et al. 2000c). Metzger et al. (2000) later reported that HST/STIS imaging of the field revealed that the OT was location was $0''.08 \pm 0''.15$ east of the center of the optically bright component, a compact galaxy. For our astrometry we used an early Keck R -band image and late I -band image, an identified 40 astrometric tie objects. At the epoch of the late I -band measurement, Bloom et al. (2000c) reported that the light curve already began to level-off, suggesting at least $\sim 80\%$ of the flux was from the compact host galaxy. The result is an improvement in the uncertainties by a factor of ~ 5 over the Metzger et al. (2000) analysis. Within errors, the OT is consistent with the center of the host.

6. The Observed Offset Distribution

6.1. Angular Offset

As seen in Table 2 and §5, there are 20 GRBs for which we have a reliable offset measure from self-HST, HST→HST, HST→GB, GB→GB, or VLA→GB astrometric ties. There are several representations of this data worth exploring. In Figure 3 we plot the angular distribution of GRBs

about their presumed host galaxy. In this Figure and in the subsequent analysis we exclude GRB 980425 because the association this GRB with SN 1998bw is still controversial. And more importantly (for the purposes of this paper) the relation of GRB 980425 with the classical “cosmological” GRB is unclear (Schmidt 1999) given that, if the association proved true, the burst would have been underluminous by a factor of $\sim 10^{-5}$ (Galama et al. 1998; Bloom et al. 1998).

The offsets labeled with a question mark are from GRB 980326 and GRB 000301C, which do not have an obvious host galaxy. The offsets for these two bursts are taken with respect to the nearest galaxy detected in the field (see the discussions in §5). Indeed, if GRBs are associated with a normal galaxy population, it is not surprising that $\sim 10\%$ of GRB hosts are undetected to the $R \sim 28$ mag level (cf. Mao & Mo 1998). Indeed we believe that deeper HST imaging of these two field will reveal a faint host near the OT position. For the purposes of the probability analysis which follows we will first exclude GRB 980326 and GRB 000301C from the analysis and then show that the inclusion of GRB 980326 and GRB 000301C does not substantially change the results.

For the remaining, five bursts appear well displaced ($\gtrsim 0''.3$) from the center of their host at a high level of significance. Four additional bursts (GRB 970828, GRB 980329, GRB 981226, GRB 990506) have uncertainties large enough such that they could reasonably be located within $0''.3$ of their host. In light of the discussion in §4.0.7 it is not surprising that the astrometry of these four bursts involved absolute astrometric comparisons of a radio afterglow position with the host optical position. The median projected offset of the 19 GRBs in our sample is 0.36 arcsec.

As discussed in Appendix A, GB→GB or GB→HST astrometry could systematically suffer from the effects of differential chromatic refraction (DCR), albeit on the 5–10 mas level. The HST→HST measured offsets of GRB 970228, GRB 970508, GRB 990123, GRB 990510, GRB 990712 are immune from DCR effects. Since optical transients are, in general, red in appearance and their hosts blue, DCR will systematically appear to pull OTs away from their hosts in the direction of the horizon. Comparing the observed offsets directions direction of the horizon at the time of each OT observation in Table 2, we find no systematic correlation thus confirming that DCR does not appear to play a dominate role in determining the differential offsets of OTs from their hosts.

What is the probability that GRBs are not associated with galaxies, *i.e.*, that, by random chance 19 positions on the sky could have a similar offset distribution as observed? We could treat each offset as a probability separately but this would require making several *a posteriori* assumptions for each individual case (e.g., the detection limits of the host discovery image). Instead, for statistical purposes, we treat the entire distribution together and make two conservative assumptions: (1) all GRBs lie within $2''$ of a galaxy which is (2) brighter than $R = 28$ mag. This very faint magnitude level was chosen because it is, ultimately, our detection limit for assigned hosts (see §5). The density of $R \lesssim 28$ mag (or $R_{AB} \lesssim 28.2$ mag) galaxies on the sky is, as found in Gardner et al. (2000), $\approx 1.0 \times 10^6$ gal deg $^{-2}$, or 0.077 gal arcsec $^{-2}$. Therefore, within a distance of $2''$ from any

point we expect on average 0.97 galaxies. The probability⁶ of observing at least one galaxy within $2''$ of 19 random locations on the sky by random chance is $P = (1 - \exp(-0.97))^{19} = 1 \times 10^{-4}$. We consider this an extreme and thereby robust upper-limit to the true probability since 1) most GRB hosts are significantly brighter than $R = 28$ mag (so the density of field galaxies is lower) and, 2) most GRBs are found much closer than 2 arcseconds from a galaxy (Table 2).

The certainty of our host assignment of the nearest galaxy to a GRB finds added strength by using redshift information. In *all* cases where an absorption redshift is found in a GRB afterglow (GRB 970508, GRB 980613, GRB 990123, GRB 990510, GRB 990712, GRB 991216) the highest redshift absorption system is observed to be the same emission redshift of the nearest galaxy. Therefore, with these bursts, clearly the nearest galaxy cannot reside at a higher redshift than the GRB. The galaxy may simply be a foreground object which gives rise both to nebular line emission and the absorption of the afterglow originating from a higher redshift. However, using the observed number density evolution of absorbing systems, Bloom et al. (1997) calculated that statistically in $\gtrsim 80\%$ of such absorption cases, the GRB could reside no further than 1.25 times the absorption redshift. For example, if an emission/absorption system is found at $z = 1.0$ then there is only a $\lesssim 20\%$ chance that the GRB could have occurred beyond redshift $z = 1.25$ without another absorption system intervening. Though this argument cannot prove that a given GRB occurred from assigned host, the effect of absorption/emission redshifts is to confine the possible GRB redshifts to a shell in redshift-space, reducing dramatically the number of galaxies that could possibly host the GRB, and increasing the chance that the host assignment is correct. Since every absorption redshift measured is the same as the emission redshift, it is natural to extend this argument to the other GRBs for which no absorption redshift was measured. Given this argument and the statistical formulation above, we proceed with the hypothesis that, as a group, GRBs are indeed physically associated with galaxies assigned as hosts.

6.2. Physical Projection

Of the 19 GRBs with offsets five have no confirmed redshift; therefore it is not immediately possible to set a physical scale to the angular distribution depicted in Fig. 3. Given the apparent angular extent of the host of GRB 990705, however, the GRB likely occurred at redshift $z \approx 0.15\text{--}0.35$. So the physical scale as a function of angular displacement (D_θ ; Table 1) for GRB 990705 is reasonably $2.8\text{--}5.3$ kpc arcsec $^{-1}$. For purposes of plotting the physical offset of GRB 990705 alongside the others we assign $D_\theta(z = 0.25) = 4.2 \pm 1.0$ kpc arcsec $^{-1}$. The other four bursts have hosts fainter than $R \approx 25$ mag and will likely fall in the redshift range $z = 0.5\text{--}5$. It is interesting to note (with our assumed cosmology) that despite a luminosity distance ratio of 37 between these two redshifts, the angular scales are about the same: $D_\theta(z = 0.5)/D_\theta(z = 5) \approx 1$.

⁶We neglect that galaxies are clustered in formulating this probability, which, since observed angular clustering decreases with increasing magnitude (cf. Fynbo et al. 2000a), is reasonable.

In fact over this entire redshift range, $6.6 \text{ kpc arcsec}^{-1} < D_\theta(z) < 9.1 \text{ kpc arcsec}^{-1}$ which renders the conversion of angular displacement to physical projection relatively insensitive to redshift. For these four bursts, then, we assign the median D_θ of the other bursts with known redshifts so that $D_\theta = 8.552 \text{ kpc arcsec}^{-1}$ (corresponding to a redshift of $z = 0.966$) and scale the observed offset uncertainty by an additional 30%. Here, we use the GRB redshifts (and, below, host magnitudes) compiled in the review by Kulkarni et al. (2000). The resulting physical projected distribution is depicted in Figure 3 and given in Table 1. The median preprojected physical offset of the 19 GRBs in the sample is 3.1 kpc.

6.3. Host-Normalized Projected Offset

If GRBs were to arise from merging remnants then galaxies of higher mass would more readily retain the progenitors and GRBs from massive galaxies would then appear to occur at systematically smaller offsets. We can try to remove the physical offset dependence on host mass by scaling each observed offset by an effective radius (R_{half} in Table 3) of the host. Table 3 shows the angular offsets and the effective radius used for scaling. In a handful of HST/STIS images of host galaxies with high signal-to-noise detections, the effective radius (taken as half-light radius) of the host can be directly measured (col. 2, Table 3). Where no half-light radius is available from direct imaging we use the median half-light radius estimated from the empirical magnitude-half-light radius relation of Odewahn et al. (1996). Further, we assign an uncertainty of 30% to these statistical estimates of R_{half} . The resulting distribution is depicted in Figure 4. The choice of cosmology does not affect the host-normalized offset.

Given the small-number statistics and a range in relative uncertainties in the offsets of the individual cases it is not strictly appropriate to construct a histogram of the data to access the probability of a burst occurring at some projected distance from its host. A histogram would require an arbitrary binning and, in some cases, the bin widths could be smaller than the error on individual measurements. Cumulative histograms also give undue weight to measurements where the errors are large, essentially assuming that each measurement is a δ -function at a given offset irrespective of the significance of each measurement.

To this end we have developed a method to construct a probability histogram (PH) that takes into account the errors on the measurements. Simply put, we treat each measurement as a probability distribution of offset (rather than a δ -function) and create a smooth histogram by summing over all GRB probability distributions. We derive the PH distribution in Appendix B. For each offset i we create an individual PH distribution function, $p_i(r) \text{ d}r$, representing the probability of observing a host-normalized offset r for that burst. The total PH is then constructed as $p(r) \text{ d}r = \sum_i p_i(r) \text{ d}r$ and plotted as a shaded region curve in 6. Each $p_i(r) \text{ d}r$ is normalized to unity so that each burst gets equal weighting. The usual histogram representation and the total probability histogram $\int_0^r p(r) \text{ d}r$ is depicted as the solid smooth curve in Figures 5. There is, as expected, a qualitative similarity between the cumulative total PH distribution and the usual cumulative

histogram distribution.

7. Testing Progentior Model Predictions

Given the observed offset distribution, we are now in the position to ask the question: which progenitor models are favored by the data the distribution? Clearly, GRBs as a class do not appear to reside at the centers of galaxies and so we can essentially rule out the possibility that *all* GRBs localized to date arise from nuclear activity. In the following analysis, we exclude offsets derived for the two GRBs with uncertain hosts (GRB 980326 and GRB 000301C), and later show the results do not change significantly by including the two “offsets”.

7.1. Delayed Merging Remnants Binaries (BH–NS and NS–NS)

As noted in the introduction, individual offsets themselves already have been shown qualitatively to pose difficulty for merging remnant models, especially those bursts with small angular offsets from undermassive galaxies (e.g., GRB 970508: Bloom et al. 1998; Paczyński 1998). Several groups predicted the distribution of *linear* distances traveled by NS–NS systems until coalescence. However, what we require is the expected radial distribution about galaxy centers. This can be obtained by integrating the motion of the binary remnant system within realistic galactic potentials and recording the locations where the binary systems merge. Bloom et al. (1999b), Fryer et al. (1999) and Bulik et al. (1999) all computed the expected radial distribution in this manner and found the offset distribution of NS–NS mergers about galaxies of a variety of galactic masses. All three studies essentially agree on the NS–NS differential offset distributions as a function of host galaxy mass. (Note that the displayed distance axis, when compared to the differential distribution, is erroneously too large by a factor of ten plot in the *cumulative* offset prediction plot in Fig. 22 of Fryer et al. 1999.) Fryer et al. (1999) point out that the Bloom et al. (1999b) synthesis appears to have incorrectly predicted an overabundance of compact binaries with small merger ages, because the population synthesis did not include a nonzero helium star radius.

The formation scenarios of BH–NS binaries are less certain than of NS–NS binaries. Both Fryer et al. (1999) and Belczyński et al. (2000) suggest that so-called “hypercritical accretion” (Bethe & Brown 1998) dominates the birthrate of BH–NS binaries. Briefly, hypercritical accretion occurs when the primary star evolves off the main sequence and explodes as a supernova, leaving behind a neutron star. Mass is rapidly accreted from the secondary star (in red giant phase) during common envelope evolution, causing the primary neutron star to collapse to a black hole. The secondary then undergoes a supernova explosion leaving behind a NS. As in NS–NS binary formation, only some BH–NS systems will remain bound after having received systemic velocity kicks from two supernovae explosions. One important difference is that BH–NS binaries are in general more massive (total system mass $M_{\text{tot}} \approx 5M_{\odot}$) than NS–NS binaries ($M_{\text{tot}} \approx 3M_{\odot}$). Furthermore,

the coalescence timescale after the second supernova is shorter than in NS–NS binaries because of the BH mass. Therefore, despite similar evolutionary tracks BH–NS binaries should be retained more tightly to host galaxies than NS–NS binaries (Bloom et al. 1999b; Belczyński et al. 2000). Belczyński et al. (2000) quantified this expected trend, showing that on average, BH–NS binaries merge \sim few times closer to galaxies than NS–NS binaries. Surprisingly, Fryer et al. (1999) found that BH–NS binaries merged *further* from galaxies than NS–NS binaries, but this result was not explained by Fryer et al. (1999). Nevertheless, just as with NS–NS binaries, a substantial fraction of BH–NS binaries will escape the potential well of the host galaxy and merge well-outside of the host. For example, even in massive galaxies such as the Milky Way, these studies show that roughly 25% of mergers occur > 100 kpc from the center of a host galaxy.

Before comparing in detail the predicted and observed distributions, it is illustrative to note that the observed distribution appears qualitatively inconsistent with the delayed merging remnant binaries. All the population synthesis studies mentioned thus far find that at least 50% of merging remnants will occur outside of ≈ 10 kpc when the mass of the host is less than or comparable to the mass of the Milky Way. Comparing this expectation with Fig. 3, where only 2 bursts *could* lie beyond 10 kpc from their host (GRB 980326 and GRB 000301C), the simplistic Poisson probability that the observed distribution is the same as the predicted distribution is no larger than 2×10^{-3} .

To provide a more quantitative comparison of the observed distribution with the merging remnant expectation, we make two conservative assumptions all of which *serve to increase the probability that the observed set derives from the predicted distribution*. First, even though most GRB host galaxies (e.g., GRB 970508, GRB 970228, GRB 980703) are probably much less massive than our Galaxy, we compare the observed offset distribution with the expected radial distribution from galaxies with run “e” of Bloom et al. (1999b) which is in reasonable agreement with the $M = M_{\text{MilkyWay}}$ distributions of Fryer et al. (1999) (NS–NS and BH–NS), Bulik et al. (1999) (NS–NS) and Belczyński et al. (2000) (BH–NS). Mergers around smaller mass galaxies are generally further from the galaxy center since binaries can more readily escape the weaker gravitational potential. Second, we project the predicted *radial* distribution by dividing each offset by a factor of 1.15 since the projection of a merger site on to the plane of the sky results in a smaller observed distance to the host center than the radial distance. We determined the projection factor of 1.15 by a Monte Carlo simulation projecting a 3-dimentional (3-D) distribution of offsets onto the sky. The median projected offset is 87% of the 3-D radial offset. This projection of the predicted radial distribution is an arbitrary global correction. The distributions are compared in Figure 7. The one-sided Kolmogorov-Smirnov (KS) probability that the observed sample derives from the same predicted distribution is $P_{\text{KS}} = 6.8 \times 10^{-4}$. Since we have used the predicted distribution from massive host galaxies for comparison instead of the undermassive galaxy prediction (as might seem more reasonable for GRB hosts), the true probability is likely even smaller.

7.2. Massive Stars (Collapsars) and Promptly Bursting Binaries (BH–WD, He–He)

As discussed, collapsars produce GRBs in star-forming regions, as will He–He and BH–WD binaries. The localization of GRB 990705 to a spiral arm is, of course, tantalizing large-scale evidence of the GRB–star-formation connection. Ideally, however, the burst sites of individual GRBs could be studied in detail with imaging and spectroscopy and should, if the collapsar/promptly bursting binary origin is corrected, reveal that the burst sites are HII regions. Unfortunately, the GRB distances preclude a detailed examination of the specific birthsite at the tens of pc scale resolution (the typical size for a star-forming region). Weaker evidence for a star-formation connection exists in that no GRB to date has been observed to be associated with an early-type galaxy (morphologically or spectroscopically), though in practice it is often difficult to discern galaxy type with the data at hand. Indeed most well-resolved hosts appear to be compact star forming blue galaxies, spirals, or morphological irregulars.

Rather than study individual GRB burst sites, we must use the observed *distribution* of offsets and compare it with the location of star-formation in the host galaxies. Of course the (projected) radial distribution of star-formation is dependent on galaxy type, age, and merger history of the galaxy. Therefore, to unify the offset distribution, we require an assumption about the general location of star formation in galaxies. Of many GRB hosts observed and well-detected with HST (e.g., GRB 970508, GRB 971214, GRB 980703), our preliminary analysis shows that the surface brightness profile can be fit by an exponential disk. We use this as the point of departure for a simplifying assumption about all GRB hosts: we assume an exponential disk profile such that the surface brightness of the host galaxy scales linearly with the galactocentric radius in the disk. We further assume that the star formation rate of massive stars scales with the observed optical light of the host; this is not an unreasonable assumption given that HST/STIS imaging probes restframe UV light, an excellent tracer of massive stars, at GRB redshifts. Again, clearly not all host galaxies are disk-like (Fig. 2) so this assumption is not strictly valid in all cases. If r_e is the disk scale length, the half-light radius of a disk galaxy is $R_{\text{half}} = 1.67 \times r_e$, so that the simplistic model of the number density of massive star-formation regions in a galaxy is,

$$N(r) dr \propto r \exp(-1.67 r) dr, \quad (1)$$

where $r = R/R_{\text{half}}$. We make an important assumption when comparing the observed distribution with the star-formation disk model: that each GRB occurs in the disk of its host (see discussion below). Dividing the observed offset by the apparent half-light radius host essentially performs a crude deprojection.

We find the probability that the observed distribution could be derived from the simplistic distribution of massive star regions (eq. 1) is $P_{\text{KS}} = 0.52$, that is the two distributions are consistent. In Appendix C we show that these results are robust even though the uncertainties on the measurements are different for each GRB.

8. Discussion and Summary

We have determined the observed offset distribution of GRBs by astrometrically comparing localizations of GRB afterglow with optical images of the field surrounding each GRB. In 17 out of 19 cases, the GRB location appears “obviously” associated with a galaxy—either because the position is superimposed atop with a galaxy or very near ($\lesssim 1.5''$) a galaxy in an otherwise sparse field. For the 2 out of 19 GRBs without an obvious host, for the purposes of uniformity, we assign the nearest detected galaxy. In fact, irrespective of the validity of individual assignments of hosts, the offset distribution may be considered a distribution of GRB positions from the nearest respective galaxy at least as bright as $R \approx 28$ (note that in most cases the host galaxies are much brighter, typically $R = 24\text{--}26$ mag). We find that the probability that the distribution of these locations are consistent with a random distribution of galaxies on the sky is $P < 1 \times 10^{-4}$.

Using this result, we are reasonably assured that most GRB locations (excepting, likely, GRB 980326 and GRB 000301C) are correctly paired with their true host galaxy. With this assumption we then compare the distribution of GRB locations about their hosts with the *predicted* radial offset distribution of merging binary remnants. This comparison is complicated by an unknown projection factor for each burst: if a GRB occurs near an edge-on disk galaxy there is not a model independent manner to determine the true 3-D radial offset of the GRB from the center of the host. Indeed, in a few cases (e.g., GRB 980519, GRB 991216) even the “center” of the host is not well defined and we must estimate a center visually. In all other cases, we find the centers using a luminosity-weighted centroid surrounding the central peak of the putative host.

To compare the GRB offsets with those predicted by the NS–NS and NS–BH binary models, we make a general assumption about the projection factor and, to facilitate a comparison in physical units (that is, kpc offsets), we assign redshifts to the 5 hosts without a confirmed distance (§6.2). We have shown that the conversion of angular offset to physical projection is relatively insensitive to the assignation of redshift. Even with the conservative assumptions which would serve to *raise* the probability of association, we estimate that the probability that the observed GRBs offset distribution is that same as the predicted distribution of NS–NS and BH–NS binaries is $P \lesssim 10^{-3}$: that is, the observed distribution of offsets is inconsistent with delayed merging remnants at better than the 3σ level. Insofar as the observed distribution is representative (see below) and the predicted distribution is accurate, this analysis statistically renders BH–NS and NS–NS progenitor scenarios unlikely for long-duration GRBs.

Having cast doubt on the merging remnant hypothesis, we now test whether the offset distribution is consistent with the collapsar (or BH–WD, He–He) class. Since massive stars explode where they are born, we have compared the observed GRB offset distribution with a simplistic model for where massive stars are formed in late-type galaxies: an exponential disk. After normalizing each GRB offset by their host half-light radius we compare the distribution with a KS test and find remarkable agreement: $P_{\text{KS}} = 0.52$. Including the GRBs with uncertain host assignments (GRB 000301C and GRB 980326) in the analysis, $P_{\text{KS}} = 4.5 \times 10^{-3}$ (delayed merging binaries) and

$P_{KS} = 0.27$ (collapsar/promptly bursting binaries); that is, though statistically weaker, the results and conclusions above are unchanged.

This close statistical relationship of observed GRB offsets with disks and massive star formation is qualitatively corroborated by inspection of the location of GRBs with respect to the apparent semi-major axis their hosts in Fig. 2. In *every* case where the host has a preferred axis and the GRB is significantly offset from the center (GRB 971214, GRB 980519, GRB 980613, GRB 980703, GRB 990510, GRB 991208), the GRB location is consistent with a location on the major axis. This observation is natural in the collapsar and promptly merging remnants but difficult to reconcile in the late merging remnant models.

Thus far we have neglected discussion of the observational biases that have gone in the localization of these 19 GRBs. The usual problems plaguing supernova detection, such as the brightness of the central region of the host and dust obscuration, are not of issue for detection of the *prompt* high-energy emission (*i.e.*, X-rays and γ -rays) of GRBs since the high-energy photons will penetrate dust. If the intrinsic luminosity of GRBs only a function of the inner-workings of the central engine (that is, GRBs arise from internal shocks and not external shocks) then the luminosity of a GRB is independent of ambient number density. Therefore, prompt X-ray localizations from BeppoSAX and γ -ray locations from the IPN should not be a function of the global properties of GRB environment; only intrinsic GRB properties such as duration and hardness will affect the prompt detection probability of GRBs.

The luminosity of the afterglow is, however, surmised to be a function of the ambient number density. Specifically, the afterglow luminosity will scale as \sqrt{n} where n is the number density of hydrogen atoms in the 1–10 pc region surrounding the GRB explosion site (cf. Mészáros et al. 1998). While $n \approx 0.1\text{--}10 \text{ cm}^{-3}$ in the interstellar medium, the ambient number density is probably $n \approx 10^{-4}\text{--}10^{-6}$ in the intergalactic medium. Thus GRB afterglow in the IGM may appear $\sim 10^{-3}$ times fainter than GRB afterglow in the ISM (and even more faint compared to GRBs that occur in star-forming regions where the number densities are higher than in the ISM).

If only a small fraction of GRBs localized promptly in X-rays and studied well at optical and radio wavelengths were found as afterglow, the ambient density bias may be cause for concern. However, this is not the case. As of November 1999, 23 of 26 bursts localized by prompt emission were later found as X-ray, optical, and/or radio afterglow (cf. Frail et al. 2000a); almost all GRBs have detectable X-ray afterglow. We believe that non-detections of GRB afterglow at optical/radio wavelengths are due to instrument sensitivities. In fact, if instead the non-detections are due to strong local dust extinction, then the fraction of optically obscured GRBs are likely to be centrally biased. This is because column densities are strongest in star-forming regions and giant molecular clouds, and thus any optically obscured GRBs are preferentially located in the disk. Thus, we do not believe the ambient density bias plays any significant role in causing GRBs to be localized preferentially closer to galaxies; in fact, the opposite may be true.

The excellent agreement between our simplistic model for the location of massive stars and the

observed distribution is one of the strongest arguments yet for a collapsar (or promptly bursting binaries) origin of long-duration GRBs. However, the concordance of the predicted and observed distributions are necessary to prove the connection, although not sufficient. Obviously, there are other astrophysical distributions which could also be consistent. The presence of GRB 970508 so close to its host center (~ 90 pc), for instance, could signify multiple progenitors classes (such as an AGN origin of some small fraction of GRBs). Alternatively, the closeness could signify that our simplistic model for star-formation requires modification; in fact, in the Galaxy, star formation as a function of Galactocentric radius does not follow a pure exponential disk, but is vigorous near the center and is strongly peaked around $R \sim 5$ kpc (cf. Kennicutt 1989). As more offsets are amassed, these subtler possibilities may be addressed.

The authors thank the generous support of the staff of the W. M. Keck Foundation and the staff at the Palomar Observatories. We thank the members of the Caltech-NRAO-CARA GRB collaboration and P. van Dokkum, K. Adelberger, and R. Simcoe for helpful discussions. We thank N. Masetti for allowing us access to early ground-based data on GRB 990705. This work was greatly enhanced by the use of data taken as part of the *A Public Survey of the Host Galaxies of Gamma-Ray Bursts* with HST (#8640; S. Holland, P.I.). JSB gratefully acknowledges the fellowship from the Fannie and John Hertz Foundation. SGD acknowledges partial support from the Bressler Foundation. SRK acknowledges support from NASA and the NSF.

REFERENCES

Akerlof, C. *et al.* . 1999, Nature, 398, 400

Alcock, C. *et al.* . 1999, ApJ, 521, 602

Anderson, J. and King, I. R. 1999, PASP, 111, 1095

Bartunov, O. S., Tsvetkov, D. Y., and Filimonova, I. V. 1994, PASP, 106, 1276

Belczyński, K., Bulik, T., and Zbijewski, W. 2000, A&A, 355, 479

Bethe, H. A. and Brown, G. E. 1998, ApJ, 506, 780

Bloom, J. S. 1999, GCN notice 756; <http://gcn.gsfc.nasa.gov/gcn/>

Bloom, J. S., Diercks, A., Kulkarni, S. R., *et al.* . 2000a, GCN notice 480

Bloom, J. S., Djorgovski, S. G., and Kulkarni, S. R. 2001, submitted to ApJ; astro-ph/0007244

Bloom, J. S., Djorgovski, S. G., Kulkarni, S. R., and Frail, D. A. 1998, ApJ, 507, L25

Bloom, J. S. *et al.* . 1998, ApJ, 508, L21

Bloom, J. S., Kulkarni, S. R., Djorgovski, S. G., Gal, R. R., Eichelberger, A., and Frail, D. A. 1998, GCN notice 149

Bloom, J. S., Kulkarni, S. R., Harrison, F., Prince, T., Phinney, E. S., and Frail, D. A. 1998, ApJ, 506, L105

Bloom, J. S., Kulkarni, S. R., *et al.* . 2000b, GCN notice 702

Bloom, J. S. *et al.* . 1999a, ApJ, 518, L1

Bloom, J. S., Sigurdsson, S., and Pols, O. R. 1999b, MNRAS, 305, 763

Bloom, J. S., Sigurdsson, S., Wijers, R. A. M. J., Almaini, O., Tanvir, N. R., and Johnson, R. A. 1997, MNRAS, 292, L55

Bloom, J. S. *et al.* . 1999, Nature, 401, 453

—. 2000c, GCN notice 689

Boella, G., Butler, R. C., Perola, G. C., Piro, L., Scarsi, L., and Bleeker, J. A. M. 1997, A&A, 122, 299

Brandt, N. and Podsiadlowski, P. 1995, MNRAS, 274, 461

Briggs, M. S., Pendleton, G. N., Kippen, R. M., Brainerd, J. J., Hurley, K., Connaughton, V., and Meegan, C. A. 1999, ApJS, 122, 503

Bulik, T., Belczyński, K., and Zbijewski, W. 1999, MNRAS, 309, 629

Carter, B. 1992, ApJ, 391, L67

Castro, S. M., Diercks, A., Djorgovski, S. G., Kulkarni, S. R., Galama, T. J., Bloom, J. S., Harrison, F. A., and Frail, D. A. 2000, GCN notice 605

Cheng, K. S. and Wang, J. 1999, ApJ, 521, 502

Chevalier, R. A. and Li, Z. 2000, ApJ, 536, 195

Cline, T. L. *et al.* . 1999, A&AS, 138, 557

Costa, E. *et al.* . 1997, Nature, 387, 783

Davis, L. 1987, <http://iraf.noao.edu/iraf/ftp/iraf/docs/apspec.ps.Z>

de Bernardis, P. *et al.* . 2000, Nature, 404, 955

Deutsch, E. W. 1999, AJ, 118, 1882

Diercks, A., Castro, S. M., Bloom, J. S., *et al.* . 2000a, in preparation

Diercks, A. *et al.* . 2000b, GCN notice 764

Djorgovski, S. *et al.* . 2000, ApJ, in preparation

Djorgovski, S. G., Bloom, J. S., and Kulkarni, S. R. 2001, submitted to ApJ Letters

Djorgovski, S. G., Gal, R. R., Kulkarni, S. R., Bloom, J. S., and Kelly, A. 1998, GCN notice 79

Eichler, D., Livio, M., Piran, T., and Schramm, D. N. 1989, Nature, 340, 126

Epps, H. W. and Miller, J. S. 1998, Proc. SPIE, 3355, 48

Esin, A. A. and Blandford, R. 2000, ApJ, 534, L151

Fenimore, E. E., Epstein, R. I., and Ho, C. 1993, A&AS, 97, 59

Fenimore, E. E., Ramirez-Ruiz, E., and Wu, B. 1999, ApJ, 518, L73

Finger, G., Biereichel, P., Mehrgan, H., Meyer, M., Moorwood, A. F., Nicolini, G., and Stegmeier, J. 1998, Proc. SPIE, 3354, 87

Fishman, G. J. and Meegan, C. A. 1995, Ann. Rev. Astr. Ap., 33, 415

Frail, D. A. *et al.* . 1999, ApJ, 525, L81

Frail, D. A., Kulkarni, S. R., Nicastro, S. R., Feroci, M., and Taylor, G. B. 1997, Nature, 389, 261

Frail, D. A. *et al.* . 2000a, to appear in the 5th Huntsville Symposium on Gamma Ray Bursts

—. 2000b, GCN notice 451

Frontera, F., Costa, E., dal Fiume, D., Feroci, M., Nicastro, L., Orlandini, M., Palazzi, E., and Zavattini, G. 1997, A&A, 122, 357

Fruchter, A., Metzger, M., Petro, L., *et al.* . 2000a, GCN notice 701

Fruchter, A. and Pian, E. 1998, GCN notice 151

Fruchter, A., Sahu, K., Gibbons, R., *et al.* . 2000b, GCN notice 575

Fruchter, A., Thorsett, S., Pian, E., *et al.* . 1999a, GCN notice 354

Fruchter, A., Vreeswijk, P., Hook, R., *et al.* . 2000c, GCN notice 752

Fruchter, A. *et al.* . 1999b, GCN notice 386

Fruchter, A. S. and Hook, R. N. 1997, in Applications of Digital Image Processing XX, Proc. SPIE, Vol. 3164, ed. A. Tescher (SPIE), 120–125

Fruchter, A. S. *et al.* . 1999, ApJ, 516, 683

Fryer, C. L. and Woosley, S. E. 1998, ApJ, 502, L9

Fryer, C. L., Woosley, S. E., and Hartmann, D. H. 1999, ApJ, 526, 152

Fukugita, M., Ichikawa, T., Gunn, J. E., Doi, M., Shimasaku, K., and Schneider, D. P. 1996, AJ, 111, 1748

Fynbo, J. P. U. *et al.* . 2000, GCN notice 570

Fynbo, J. U., Freudling, W., and Möller, P. 2000a, A&A, 355, 37

Fynbo, J. U. *et al.* . 2000b, accepted for publication in ApJ Letters

Galama, T. 1999, PhD thesis, University of Amsterdam

Galama, T. J. *et al.* . 2000, ApJ, 536, 185

—. 1998, Nature, 395, 670

Galama, T. J. *et al.* . 1999, GCN 313

Gardner, J. P. *et al.* . 2000, AJ, 119, 486

Garnavich, P. M., Loeb, A., and Stanek, K. Z. 2001, submitted to ApJ Letters

Goodman, J. 1986, ApJ, 308, 47

Groot, P. J. *et al.* . 1998a, ApJ, 493, L27

—. 1998b, ApJ, 502, L123

Gubler, J. and Tytler, D. 1998, PASP, 110, 738

Hakkila, J., Meegan, C. A., Pendleton, G. N., Briggs, M. S., Horack, J. M., Hartmann, D. H., and Connaughton, V. 1998, in Gamma Ray Bursts: 4th Huntsville Symposium, ed. C. A. Meegan, R. Preece, & T. Koshut (Woodbury, New York: AIP), 236–240

Hansen, B. M. S. and Phinney, E. S. 1997, MNRAS, 291, 569

Harrison, F. A. *et al.* . 1999, ApJ, 523, L121

Hjorth, J., Andersen, M. I., Pedersen, H., Jaunsen, A. O., Costa, E., and Palazzi, E. 1998, GCN notice 109

Hjorth, J., Holland, S., Courbin, F., Dar, A., Olsen, L. F., and Scodéglio, M. 2000, ApJ, 534, L147

Hjorth, J. *et al.* . 2000a, GCN notice 731

—. 2000b, GCN notice 749

Holland, S., Fynbo, J., Thomsen, B., *et al.* . 2000a, GCN notice 704

—. 2000b, GCN notice 698

Holland, S., M, A., and Hjorth, J. 2000c, GCN notice 793

Hurley, K. *et al.* . 2000a, GCN notice 736

—. 2000b, GCN notice 791

—. 2000c, GCN notice 801

Jager, R. *et al.* . 1997, A&AS, 125, 557

Johnson, H. M. and MacLeod, J. M. 1963, PASP, 75, 123

Kells, W., Dressler, A., Sivararamakrishnan, A., Carr, D., Koch, E., Epps, H., Hilyard, D., and Pardeilhan, G. 1998, PASP, 110, 1487

Kennicutt, R. C. 1989, ApJ, 344, 685

Kimble, R. A. *et al.* . 1998, ApJ, 492, L83

Klebesadel, R. W., Strong, I. B., and Olson, R. A. 1973, ApJ, 182, L85

Kulkarni, S. R. *et al.* . 2000, Proc. SPIE, 4005, 9

—. 1998, Nature, 393, 35

Kumar, P. 1999, ApJ, 523, L113

Lamb, D. Q. 1995, PASP, 107, 1152

Lazzati, D., Covino, S., and Ghisellini, G. 2000, to appear in the proceedings of the 5th Huntsville GRBs symposium (Huntsville AL, Oct. 1999)

Lindegren, L. 1980, A&A, 89, 41

MacFadyen, A. I. and Woosley, S. E. 1999, ApJ, 524, 262

Malumuth, E. M. and Bowers, C. W. 1997, in The 1997 HST Calibration Workshop with a new generation of instruments; eds. Stefano Casertano, Robert Jedrzejewski, Charles D. Keyes, and Mark Stevens. Baltimore, MD : Space Telescope Science Institute, 144

Mao, S. and Mo, H. J. 1998, A&A, 339, L1

Masetti, N. *et al.* . 2000, A&A, 354, 473

McLean, I. S. *et al.* . 1998, SPIE, 3354, 566

Mészáros, P., Rees, M. J., and Wijers, R. A. M. J. 1998, *ApJ*, 499, 301

Metzger, M., Fruchter, A., Masetti, N., *et al.* . 2000, GCN notice 733

Metzger, M. R., Djorgovski, S. G., Kulkarni, S. R., Steidel, C. C., Adelberger, K. L., Frail, D. A., Costa, E., and Fronterra, F. 1997a, *Nature*, 387, 879

Metzger, M. R., Kulkarni, S. R., Djorgovski, S. G., Gal, R., Steidel, C. C., and Frail, D. A. 1997b, IAU circular 6588

Mirabal, N., Halpern, J. P., Wagner, R. M., *et al.* . 2000, GCN notice 650

Monet, D. G. 1998, in American Astronomical Society Meeting, Vol. 193, 12003

Narayan, R., Paczyński, B., and Piran, T. 1992, *ApJ*, 395, L83

Nicklas, H., Seifert, W., Boehnhardt, H., Kiesewetter-Koebinger, S., and Rupprecht, G. 1997, Proc. SPIE, 2871, 1222

Odewahn, S. C., Windhorst, R. A., Driver, S. P., and Keel, W. C. 1996, *ApJ*, 472, L13

Odewhan, S. C. *et al.* . 1998, *ApJ*, 509, L5

Oke, J. B. *et al.* . 1995, *PASP*, 107, 375

Paczyński, B. 1986, *ApJ*, 308, L43

—. 1995, *PASP*, 107, 1167

—. 1998, *ApJ*, 494, L45

Phinney, E. S. 1991, *ApJ*, 380, L17

Pian, E. *et al.* . 1998, *ApJ*, 492, L103

Piran, T. 1999, *Phys. Rep.*, 314, 575

Piro, L. *et al.* . 1999, *ApJ*, 514, L73

Piro, L. *et al.* . 2001, submitted to *Science*

Portegies Zwart, S. F. and Spreeuw, H. N. 1996, *A&A*, 312, 670

Reaves, G. 1953, *PASP*, 65, 242

Rees, M. J. 1999, *A&A*, 138, 491

Reichart, D. E. 1999, *ApJ*, 521, L111

Reichart, D. E. 2001, to be submitted to *ApJ Letters*.

Sahu, K. C. *et al.* . 1997, *Nature*, 387, 476

Sahu, K. C. *et al.* . 2000, in astro-ph/0003378

Schaefer, B. E. *et al.* . 1999, *ApJ*, 524, L103

Schmidt, M. 1999, *ApJ*, 523, L117

Smette, A. *et al.* . 2001, submitted to *ApJ*

Stanek, K. Z., Garnavich, P. M., Kaluzny, J., Pych, W., and Thompson, I. 1999, *ApJ*, 522, L39

Stone, R. C. 1989, *AJ*, 97, 1227

Stornelli, M., Celidonio, G., Muller, J., Zand, J. I., Amati, L., Feroci, M., and Gandolfi, G. 2000, GCN notice 540

Taylor, G. B., Beasley, A. J., Frail, D. A., Kulkarni, S. R., and Reynolds, J. E. 1999, *A&A*, 138, 445

Taylor, G. B., Bloom, J. S., Frail, D. A., Kulkarni, S. R., Djorgovski, S. G., and Jacoby, B. A. 2000, *ApJ*, 537, L17

Taylor, G. B., Frail, D. A., and Kulkarni, S. R. 1998a, GCN notice 40

Taylor, G. B. *et al.* . 1998b, *ApJ*, 502, L115

Taylor, J. H. 1994, *Rev. Mod. Phys.*, 66, 711

Uglesich, R., Mirabal, N., Halpern, J., *et al.* . 2000, GCN notice 472

van Dyk, S. D. 1992, *AJ*, 103, 1788

van Paradijs, J. *et al.* . 1997, *Nature*, 386, 686

van Paradijs, J., Kouveliotou, C., and Wijers, R. A. M. J. 2000, to appear in *ARAA*

Vietri, M., Perola, C., Piro, L., and Stella, L. 1999, *MNRAS*, 308, L29

Vreeswijk, P. M., Fruchter, A., Ferguson, H., Kouveliotou, C., *et al.* . 2000, GCN notice 751

Vreeswijk, P. M., Galama, T. J., Rol, E., *et al.* . 1999, GCN notice 310

Wax, N., ed. 1954, *Selected Papers on Noise And Stochastic Processes* (Dover Publications, Inc.), see pg. 238

Waxman, E. and Draine, B. T. 2000, *ApJ*, 537, 796

Weth, C., Mészáros, P., Kallman, T., and Rees, M. J. 2000, *ApJ*, 534, 581

Wieringa, M. *et al.* 1998. IAU circular 6896

Wijers, R. A. M. J., Bloom, J. S., Bagla, J., and Natarajan, P. 1998, MNRAS, 294, L17

Woosley, S. E. 1993, ApJ, 405, 273

Yoshida, A., Namiki, M., Otani, C., Kawai, N., Murakami, T., Ueda, Y., Shibata, R., and Uno, S. 1999, A&A, 318, 433

A. Potential sources of astrometric error

A.1. Differential Chromatic Refraction

Ground-Based imaging always suffers from differential chromatic refraction (DCR) introduced by the atmosphere. The magnitude of the refraction depends strongly ($\propto 1/\lambda_{\text{eff}}^2$) on the effective wavelength (λ_{eff}) of each object, the airmass of the observation, and the air temperature and pressure. With increasing airmass, the stellar image is dispersed by the atmosphere and stretched pointing towards the horizon. Likewise, bluer objects appear to shift towards the zenith and redder objects towards the horizon. Since we are only concerned with the differential and systematic distortion across an image introduced in one epoch we wish to quantify only the effects of varying color and position on an exposure. Other sources of refraction, such as turbulent refraction (Lindegren 1980), are statistical in nature and will only serve to increase the uncertainty in our astrometric solution.

All of our early ground-based imaging was conducted with $\sec(z) \lesssim 1.6$ so we take as an extreme example an image with airmass image is $\sec(z) = 2$, where z is the observed angular position of the transient/host galaxy from the zenith. It is instructive to determine the scale of systematic offset shifts introduced when compared with either HST imaging or late-time imaging taken at a low or no airmass where refractive distortions are minimal. Following Gubler & Tytler (1998), the differential angular distortion between two point sources at an apparent angular separation along the zenith, Δz , is broken into a color and a zenith distance term. Assuming nominal values for the altitude of Mauna Kea, atmospheric temperature, humidity and pressure, at an effective wavelength of the R -band filter, $\lambda_{\text{eff}}(R) = 6588 \text{ \AA}$ (Fukugita *et al.* 1996), the zenith distance term is 16 mas for an angular separation of 30 arcsec at an airmass of $\sec(z) = 2$. To first order, the zenith term is linear in angular distance and so, in practice, even this small effect will be solved for in the differential mapping as a first-order perturbation to the overall rotation, translation, and scale mapping between a Keck and HST image. In other words, we can neglect the zenith term contribution to the DCR.

We now determine the color term contribution. Optical transients are in general, redder in appearance (apparent $V - R \approx 0.5$ mag) than their host galaxies (apparent $V - R \sim 0.2$ mag). Assume the average astrometric tie object has $V - R = 0.4$ mag. If the OT is observed through an airmass of $\text{sec}(z) = 1.9$ and then the galaxy is observed at a later time through an airmass of, for example, $\text{sec}(z) = 1.2$, then DCR will induce a ~ 30 mas centroid shift between the OT and the host galaxy if the two epochs are observed in B -band (cf. Fig. 2 of Alcock et al. 1999). In R -band, the filter used in almost all of our ground-based imaging for the present work, the DCR strength is about 20% smaller than in B -band because of the strong dependence of refraction on wavelength. Therefore we can reasonably assume that DCR should only *systematically* effect our astrometric precision at the 5–10 mas level. DCR could of course induce a larger *statistical* scatter in the uncertainty of an astrometric transformation between epochs since individual tie objects are not, in general, the same color and each will thus experience its own DCR centroid shift.

We can take steps in order to minimize the effects of DCR. Since the spectral response of the HST/STIS CCD is so broad, extended objects with color gradients will have different apparent relative locations when compared with our deep ground-based R -band images. As such, in choosing astrometric tie objects, we pay particular attention to choosing objects which appear compact (half-light radii $\lesssim 0''.3$) on the STIS image.

A.2. Field Distortion

Optical field distortion is another source of potential error in astrometric calibration. Without correcting for distortion in STIS, the maximum distortion displacement (on the field edges) is ~ 35 mas (Malumuth & Bowers 1997). This distortion is corrected to a precision at the sub-milliarcscale level on individual STIS exposures with IRAF/DITHER (Malumuth & Bowers 1997). Malumuth & Bowers (1997) also found that the overall plate scale appears to be quite stable with r.m.s. changes at the 0.1% level. We confirmed this result by comparing two epochs of imaging on GRB 990510 and GRB 970508 which span about 1 year. The relative plate scale of the geometric mapping between final reductions was unity to within 0.03%.

We do not correct for optical field distortion before mapping ground-based images to HST. While there may be considerable distortion ($\sim \text{few} \times 100$ mas) across whole ground-based CCD images, these distortions are correlated on small scales. Therefore, when mapping a 50×50 arcsec 2 portion of a Keck image with an HST image, the intrinsic differential distortions in the Keck image tend to be small ($\lesssim 30$ –50 mas). Much of the distortion is accounted for in the mapping by the higher-order terms of the fit, and any residual differential distortions simply add scatter to the mapping uncertainties.

B. Derivation of the probability histogram (PH)

Histogram binning is most informative when there are a many more data points than bins and the bin sizes are much larger than the errors on the individual measurements. Unfortunately, the set of GRB offsets is contrary to both these requirements. We require a method to display the data as in the traditional histogram, but where the errors on the measurements are accounted for. Instead of representing each measurement as a δ -function, we will represent each measurement as a probability distribution as a function of offset.

What distribution function is suitable for offsets? When the offset is much larger than the error, then the probability that the burst occurred at the measured displacement should approach a δ -function. When the offset is much larger than zero, then the probability distribution should appear essentially Gaussian (assuming the error on the measurement is Gaussian). However, when the observed offset is small and the error on the measurement non-negligible with respect to the observed offset, the probability distribution is decidedly non-Gaussian since the probability is only physical for positive offsets. The distribution we seek is similar to the well-known Rice distribution (cf. Wax 1954), only more general.

We derive the probability histogram (PH) as follows. For each GRB offset, i , we construct an individual probability distribution function $p_i(r) \mathrm{d}r$ of the host-normalized offset (r_i) of the GRB given the observed values for $X_{0,i}$, $Y_{0,i}$ and host half-light radius $R_{i,\text{half}}$ and the associated uncertainties. To simplify the notation in what follows, we drop the index i and let all parameters with small capitalization represent dimensionless numbers; for example, the value $x_0 = X_0/R_{\text{half}}$, where R_{half} is the host half-light radius. Without loss of generality, we can subsume (by quadrature summation) the uncertainties in the host center, the astrometric transformation, and the GRB center into the error contribution in each coordinate. We assume that these statistical coordinate errors are Gaussian distributed with σ_x and σ_y with, for example,

$$\sigma_x = \frac{X_0}{R_{\text{half}}} \sqrt{\frac{\sigma_{X_0}^2}{X_0^2} + \frac{\sigma_{R_{\text{half}}}^2}{R_{\text{half}}^2}}.$$

Therefore, we can construct the probability $p(x, y) \mathrm{d}x \mathrm{d}y$ of the true offset at some distance x and y from the measured offset location (x_0, y_0) :

$$p(x, y) \mathrm{d}x \mathrm{d}y = \frac{1}{2\pi\sigma_x\sigma_y} \exp\left[-\frac{1}{2}\left(\frac{x^2}{\sigma_x^2} + \frac{y^2}{\sigma_y^2}\right)\right] \mathrm{d}x \mathrm{d}y, \quad (\text{B1})$$

assuming the errors in the x and y are uncorrelated. This is a good approximation since, while the astrometric mappings generally include cross-terms in X and Y , these terms are usually small. If $\sigma_x = \sigma_y$, then eq. B1 reduces to the Rayleigh distribution in distance from the observed offset, rather than the host center.

The probability distribution about the host center is found with an appropriate substitution for x and y in eq. B1. In Figure 9 we illustrate the geometry of the problem. The greyscale

distribution shows $p(x, y) dx dy$ about the offset point x_0 and y_0 . Let $\phi = \tan^{-1}(y_0/x_0)$ and transform the coordinates in eq. B1 using $\psi = \phi + \theta$, $x = r \cos \psi - x_0$, and $y = r \sin \psi - y_0$. The distribution we seek, the probability that the true offset lies a distance r from the host center, requires a marginalization of $\int_\psi p_i(r, \psi) dr d\psi$ over ψ ,

$$\begin{aligned} p_i(r) dr &= \int_\psi p_i(r, \psi) dr d\psi \\ &= \frac{J dr}{2\pi\sigma_x\sigma_y} \int_0^{2\pi} \exp\left[-\frac{1}{2}\left(\frac{x(r, \psi)^2}{\sigma_x^2} + \frac{y(r, \psi)^2}{\sigma_y^2}\right)\right] d\psi, \end{aligned} \quad (\text{B2})$$

finding $J = r$ as the Jacobian of the coordinate transformation. In general, equation B2 must be integrated numerically using the observed values x_0 , y_0 , σ_x , and σ_y . The solution is analytic, however, if we assume that $\sigma_x \rightarrow \sigma_r$ and $\sigma_y \rightarrow \sigma_r$, so that,

$$\begin{aligned} p_i(r) dr &\approx \frac{r}{\pi\sigma_r^2} \exp\left[-\frac{r^2 + r_0^2}{2\sigma_r^2}\right] \int_{\theta=0}^{\pi} \exp\left[\frac{r r_0 \cos \theta}{\sigma_r}\right] d\theta dr \\ &\approx \frac{r}{\sigma_r^2} \exp\left[-\frac{r^2 + r_0^2}{2\sigma_r^2}\right] I_0\left(\frac{r r_0}{\sigma_r^2}\right) dr, \end{aligned} \quad (\text{B3})$$

where $I_0(x)$ is the modified Besel function of zeroth order and $r_0 = \sqrt{x_0^2 + y_0^2}$.

The equation B3 is readily recognized as the Rice distribution and is often used to model the noise characteristics of visibility amplitudes in interferometry; visibility amplitudes, like offsets, are positive-definite quantities. Only when $\sigma_x = \sigma_y = \sigma_r$ is the probability distribution exactly a Rice distribution, which is usually the case for interferometric measurements since the real and imaginary components of a radio wave are measured in the same manner.

Equation B2 is a generalized form of the Rice distribution but can be approximated as a Rice distribution by finding a suitable σ_r . We find that by letting,

$$\sigma_r = \frac{1}{r_0} \sqrt{(x_0 \sigma_x)^2 + (y_0 \sigma_y)^2}, \quad (\text{B4})$$

equation B3 approximates (to better than 30%) the exact form of the probability distribution in eq. B2 as long as $\sigma_x \lesssim 2\sigma_y$ (or vice versa). In Figure 10 we show two example offset probability distributions in exact and approximate form. Note that $r_0 - \sigma_r \leq r \leq r_0 + \sigma_r$ is not necessarily the 68% percent confidence region of the true offset since the probability distribution is not Gaussian. The exact form is used to construct the data representations in Figures 5–8.

C. Testing the Robustness of the KS test

How robust are the estimates of probabilities found comparing the observed distribution and the massive star class prediction? Since there are different uncertainties on each offset measurement, the KS test is not strictly the appropriate statistic to determine the likelihood that the observed

distribution could be drawn from the same underlying (predicted) distribution. One possibility is to construct synthetic sets of observed data from the model using the observed uncertainties. However, a small uncertainty (say 0.2 arcsec in radius observed to be paired with an equally small offset) which is randomly assigned to a large offset from a Monte Carlo distribution has a different probability distribution than if assigned to a small offset (since the distribution in r is only physical for positive r). Instead, we approach the problem from the other direction by using the data themselves to assess the range in KS statistics given our data. We construct $k = 1000$ synthetic cumulative physical offset distributions using the smoothed probability offset distributions $p_i(r) dr$ for each GRB. As before r is the offset in units of host half-light radius. For each simulated offset distribution k we find a set $\{r_i\}_k$ such that,

$$P[0, 1] = \int_0^{r_i} p_i(l) dl / \int_0^{\infty} p_i(l) dl,$$

where $P[0, 1]$ is a uniform random deviate over the closed interval $[0, 1]$. We evaluate the KS statistic as above for each synthetic set and record the result. Figure 8 depicts the cumulative probability distribution compared with the simple exponential disk model. The inset of the figure shows the distribution of KS statistics for the set of synthetic cumulative distributions constructed as prescribed above. In both cases, as expected, the *observed* KS probability falls near the median of the synthetic distribution. Using this distribution of KS statistics we can now assess the robustness of our comparison result: given the data and their uncertainties, the probability that the observed GRB offset distribution is the same as the distribution of star formation is $P_{KS} \geq 0.05$ in 98.2% of our synthetic datasets.

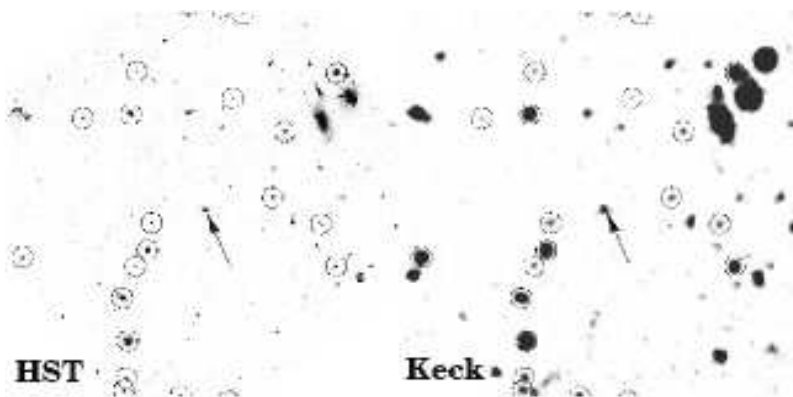


Fig. 1.— Example Keck *R*-band and HST/STIS Clear images of the field of GRB 981226. Twenty of the 25 astrometric tie objects are circled in both images. As with other Keck images used for astrometry in the present study, most of the faint object detected in the HST images are also detected (albeit with poorer resolution). The optical transient in the Keck image and the host galaxy in the HST image are in center. The field is approximately $50'' \times 50''$ with North up and East to the left. **Note: this figure shown is low resolution. To view the full-resolution image, please download the PDF version (or PS version) of the paper at <http://www.astro.caltech.edu/~jsb/Papers/offset.pdf> (.ps.gz)**

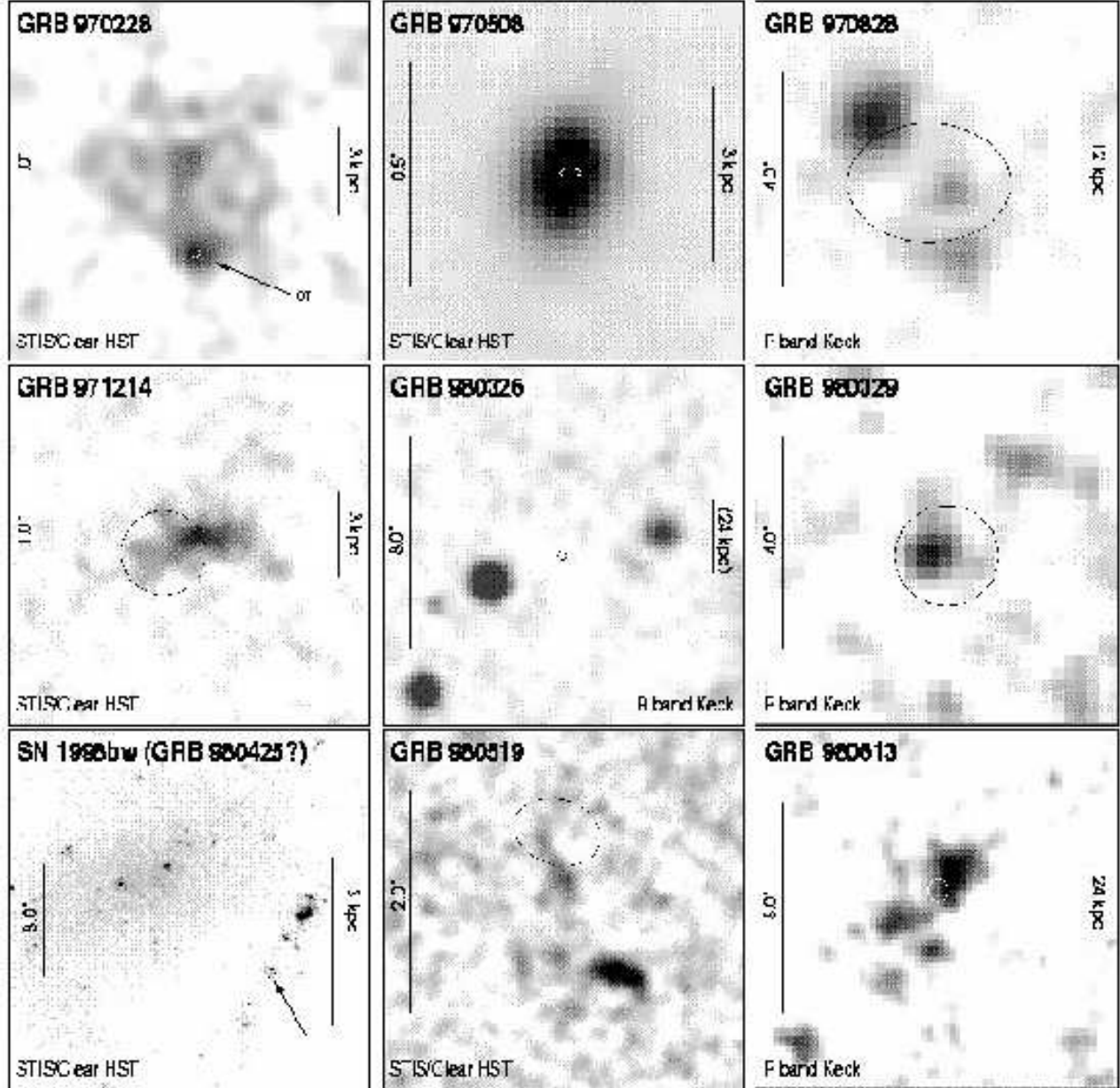


Fig. 2.— The location of individual GRBs about their host galaxies. The ellipse in each frame represents the 3σ error contour for the location of the GRB as found in §5 and in Table 2. The angular scale of each image is different and noted on the left hand side. The scale and stretch was chosen to best show both the detailed morphology of the host galaxy and the spatial relationship of the GRB and the host. In the case where we believe the true host galaxy of the GRB has yet to be detected (GRB 000301C and GRB 980326) we show a larger region of the field including the nearest detected galaxy which, in Table 2, we assign as the host. The GRB afterglow is still visible in some of the images (GRB 970228, GRB 991216, GRB 000301C). In GRB 980425, the location of the associated supernova is noted with an arrow. In all cases where a redshift is available for the host or GRB afterglow we also provide a physical scale of the region on the right hand side of each image. For all images, North is up and East is to the left. **Note: this figure shown is low resolution. To view the full-resolution image, please download the PDF (PS) version of the paper at <http://www.astro.caltech.edu/~jsb/Papers/offset.pdf> (.ps.gz)**

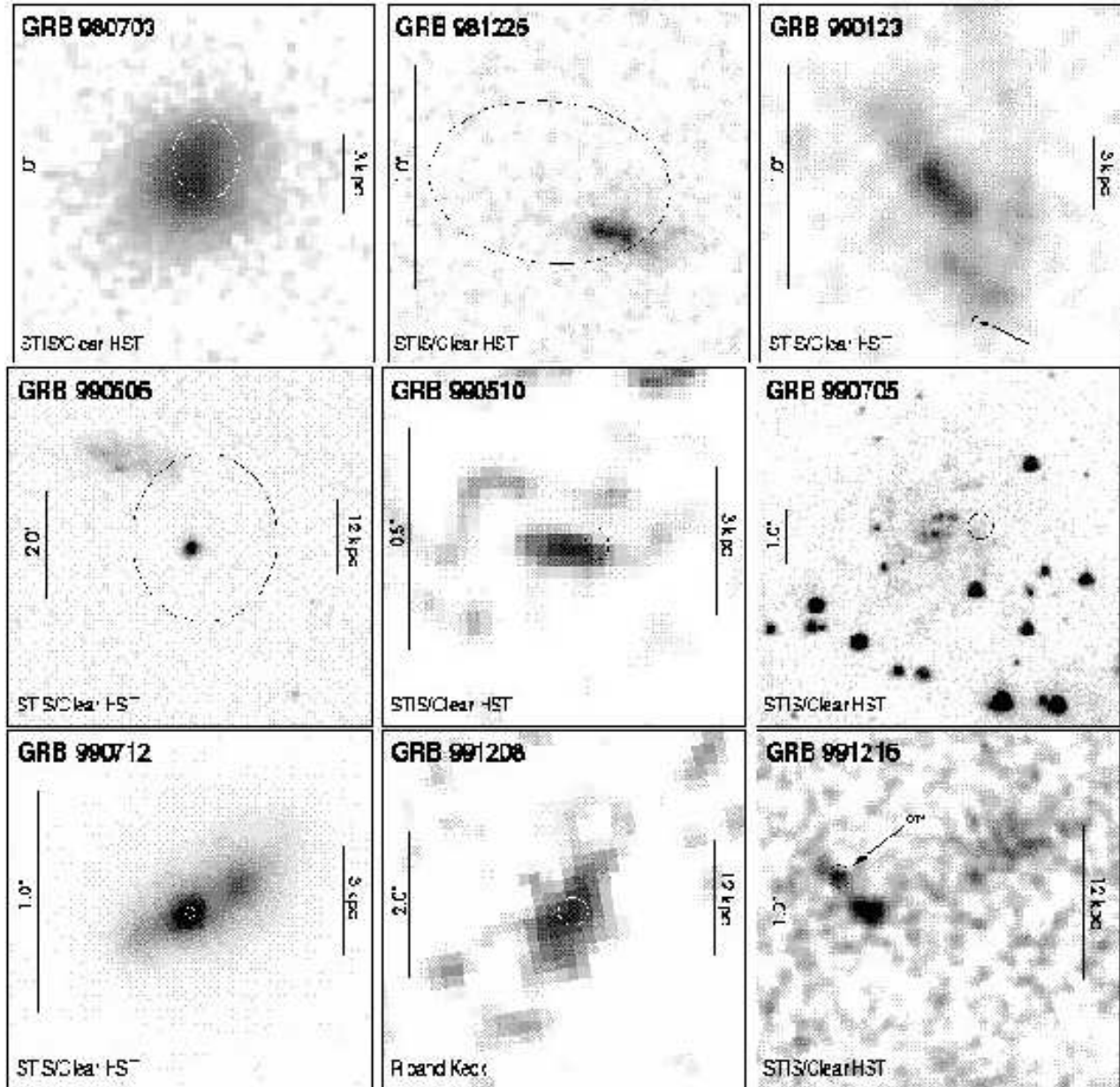


Fig. 2.— (cont.) The location of individual GRBs about their host galaxies. **Note:** this figure shown is low resolution. To view the full-resolution image, please download the PDF (PS) version of the paper at <http://www.astro.caltech.edu/~jsb/Papers/offset.pdf> (.ps.gz)

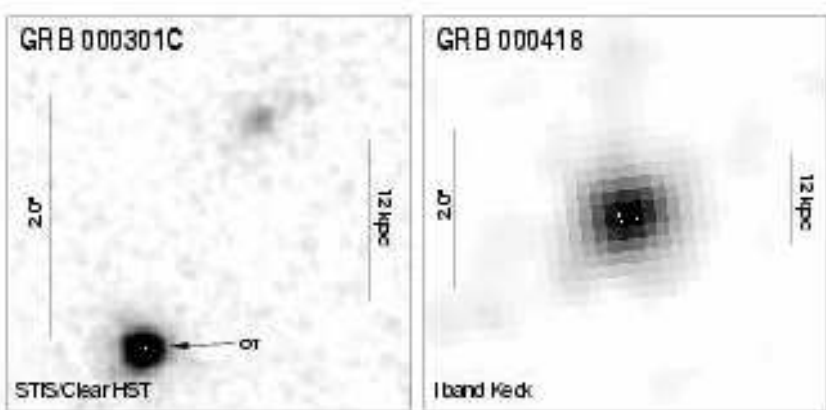


Fig. 2.— (cont.) The location of individual GRBs about their host galaxies. Note: this figure shown is low resolution. To view the full-resolution image, please download the PDF (PS) version of the paper at <http://www.astro.caltech.edu/~jsb/Papers/offset.pdf> (.ps.gz)

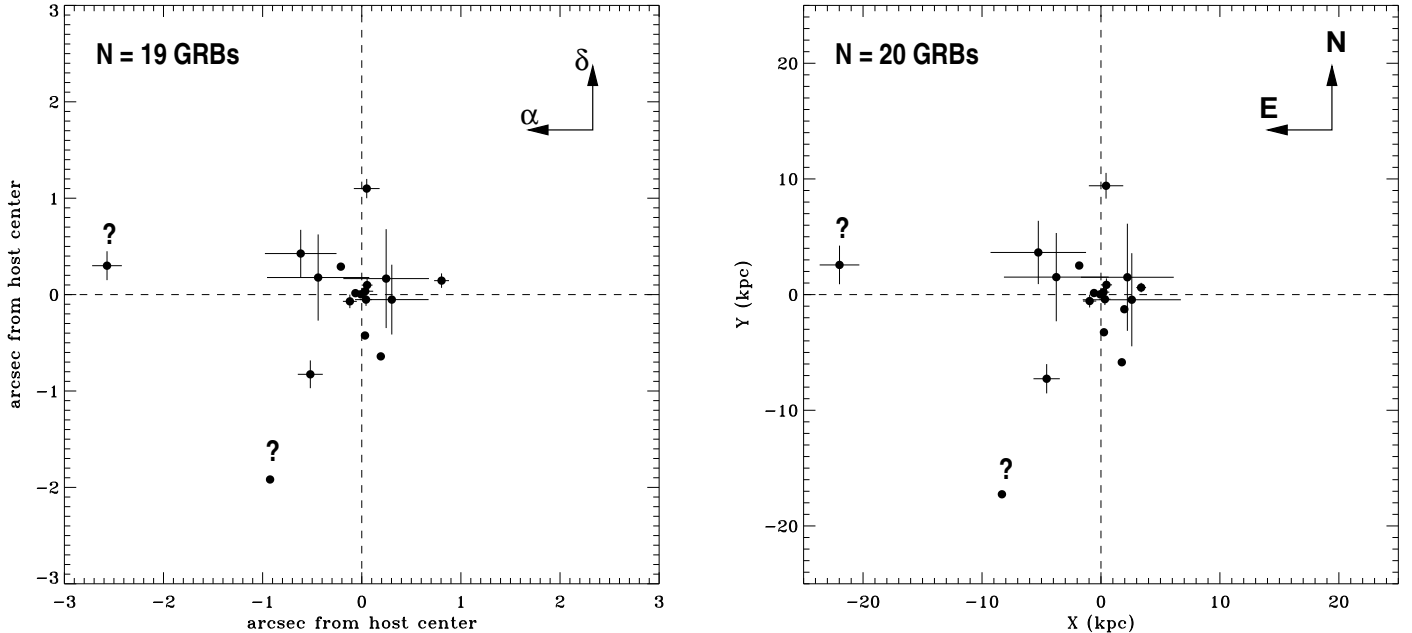


Fig. 3.— (left) The angular distribution of 19 gamma-ray bursts about their presumed host galaxy. The question marks denote the offsets of GRB 980326 and GRB 000301C assuming the nearest detected galaxy is the host (both images have detection thresholds $R_{AB} \sim 28$). The error bars are 1σ and reflect the total uncertainty in the relative location of the GRB and the apparent host center. The offset of GRB 980425 from its host is suppressed for clarity since the redshift, relative to all the others, GRB was so small. (right) The projected physical offset distribution of 20 γ -ray bursts (now including SN1998bw/GRB 980425) about their presumed host galaxies. The physical offset is assigned assuming $H_0 = 65 \text{ km/s Mpc}^{-1}$, $\Lambda = 0.7$, and $\Omega_m = 0.3$ and assuming the GRB and the presumed host are at the same redshift. Where no redshift has been directly measured a redshift is assigned equal to the median redshift ($z = 0.966$) of all GRBs with measured redshifts (see text).

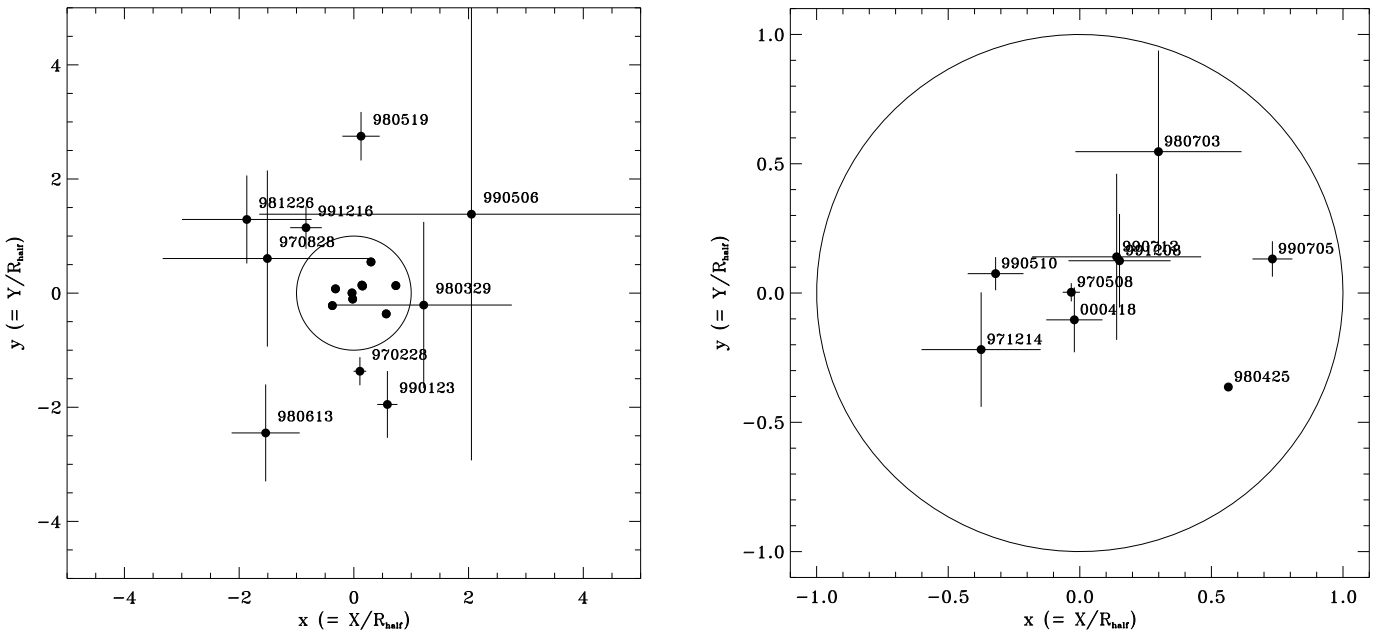


Fig. 4.— Host-normalized offset distribution. The dimensionless offsets are the observed offsets (X_0, Y_0) normalized by the host half-light radius (R_{half}) of the presumed host galaxy. See text for an explanation of how the half-light radius is found. The $1-\sigma$ error bars reflect the uncertainties in the offset measure and in the half-light radius. As expected if GRBs occur where stars are formed, there are 10 GRBs inside and 10 GRBs outside the half-light radius of their host. (left) All GRBs outside of one half-light radius (small circle) are labeled. (right) All GRBs observed to be internal to one half-light radius are labeled.

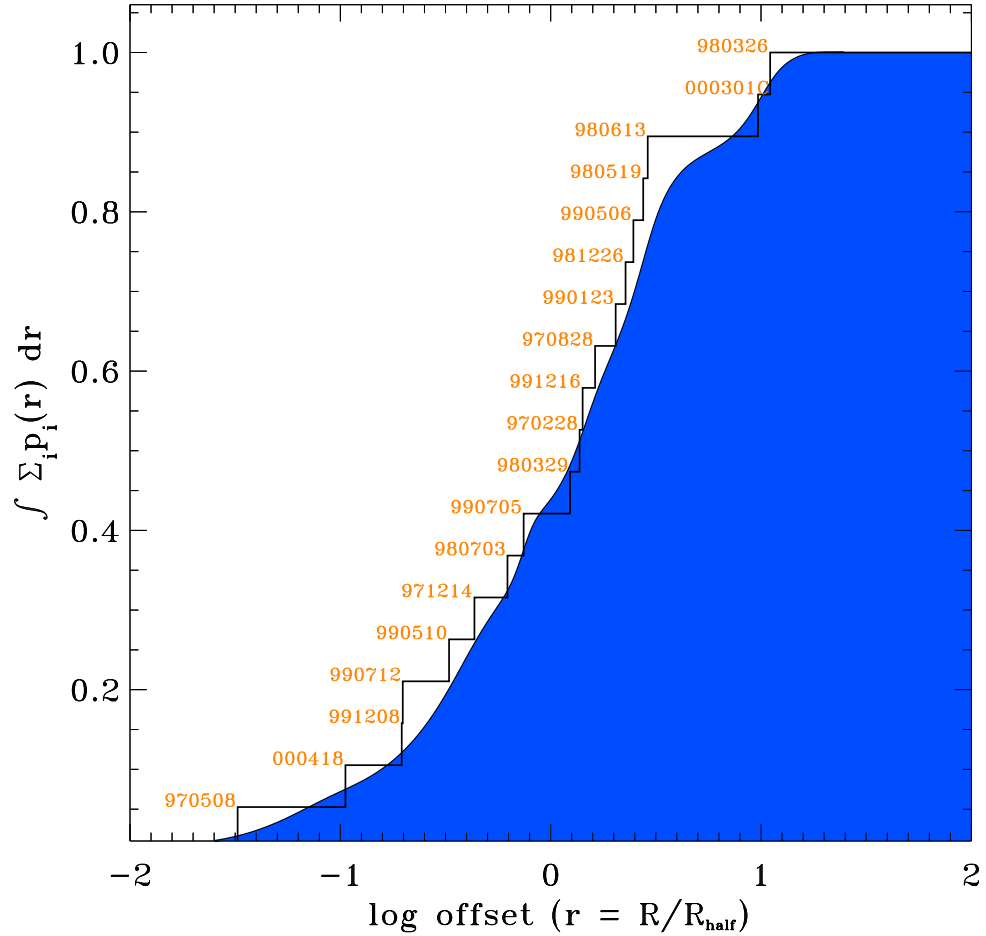


Fig. 5.— The cumulative GRB offset distribution as a function of host half-light radius. The solid jagged line is the data in histogram form. The smooth curve is the probability histogram (PH) constructed with the formalism of Appendix B and is the integral of the curve depicted in Figure 6. Notice that the histogram appears discontinuous in radius when going from GRB 980613 to the “no host” GRBs (000301C and 980326), which may imply that these two GRBs are close to hosts that have yet to be detected. The GRB identifications are noted alongside the solid histogram. In this figure and in Figure 6, GRB 980425 has not been included.

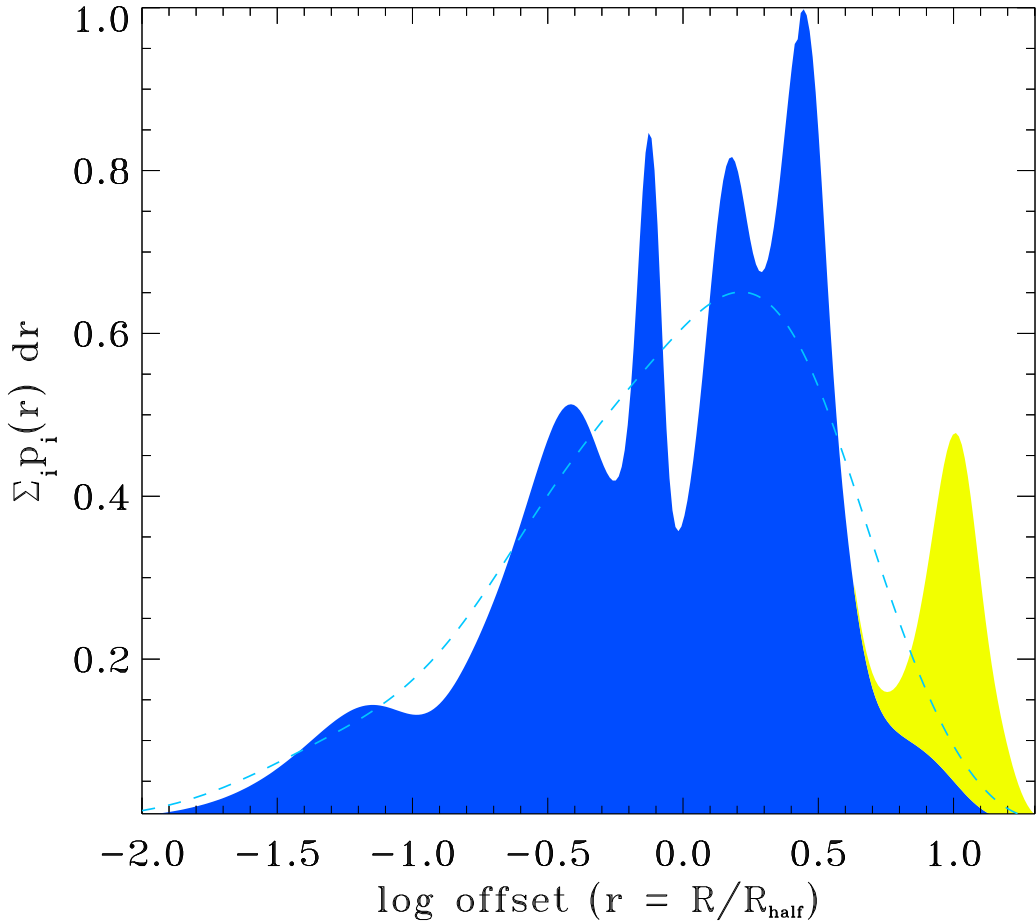


Fig. 6.— The GRB offset distribution as a function of normalized galactocentric radius. The normalized offset is $r = R/R_{\text{half}}$, where R is the projected galactocentric offset of the GRB from the host and R_{half} is the half-light radius of the host. This distribution is essentially a smooth histogram of the data but one which takes into account the uncertainties in the measurements: the sharper peaks are due to individual offsets where the significance (r_0/σ_{r_0}) of the offset is high. That is, if a GRB offset is well-determined its contribution to the distribution will appear as a δ -function centered at $r = r_0$. The yellow (light shaded) portion of the curve shows the contribution from GRB 000301C and GRB 980326. There is no obvious host for these two bursts and we choose the nearest galaxy detected as the host (see text). The dashed curve is the distribution under the blue (dark) curve but smoothed with a Gaussian of FWHM = 0.7 dex in r . Strikingly, the peak of the probability is near one half-light radius, a qualitative argument for the association of GRBs with massive star formation. We compare in detail this distribution with predicted progenitor distributions in §7.

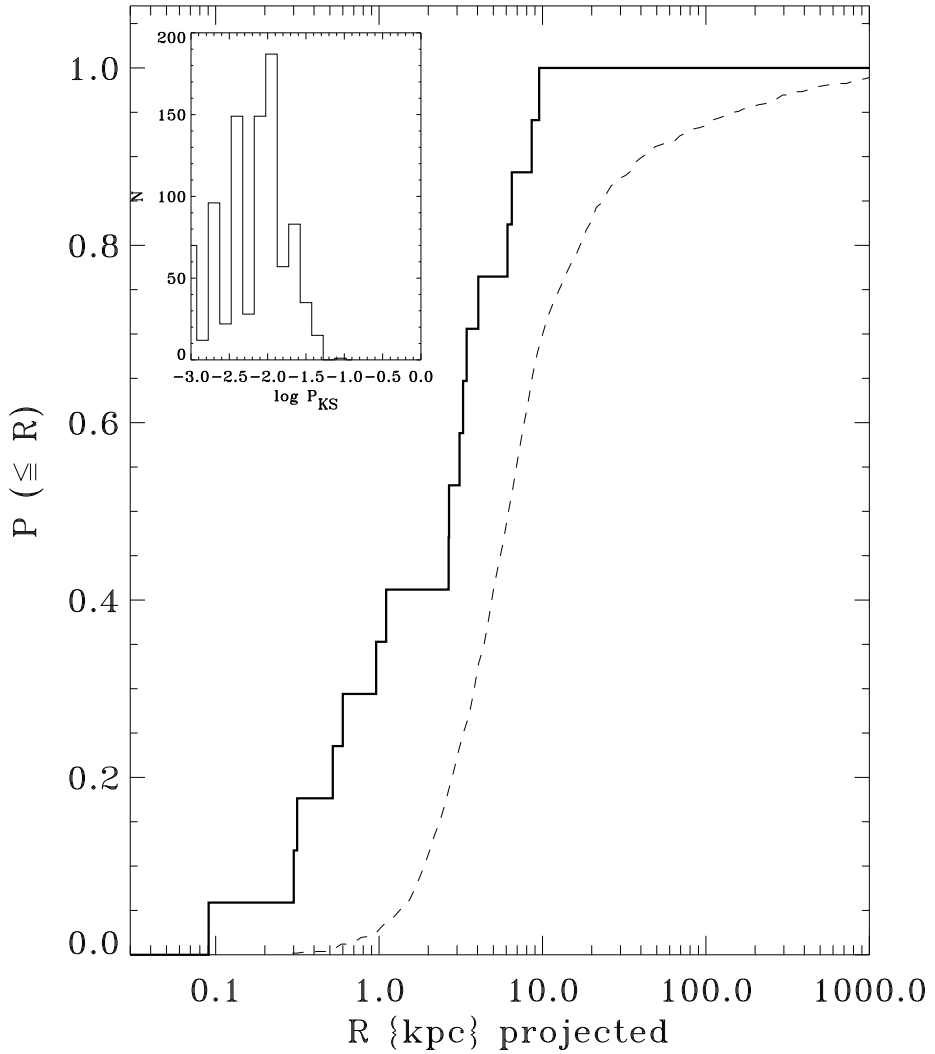


Fig. 7.— Offset distribution of GRBs compared with delayed merging remnant binaries (NS–NS and BH–NS) prediction. The model, depicted as a dashed curve, is the radial distribution from Bloom et al. (1999b) that has been projected by an average projection factor of 1.15 (see text). The cumulative histogram is the observed data set. Inset is the distribution of KS statistics (based on the maximum deviation from the predicted and observed distribution) of 1000 synthetic data sets. Even with conservative assumptions (see text) the observed GRB distribution is inconsistent with the prediction: in only 0.1% of synthetic datasets is $P_{\text{KS}} \geq 0.05$. Instead, the collapsar/promptly bursting remnant progenitor prediction is an excellent representation of the data (see Fig. 8).

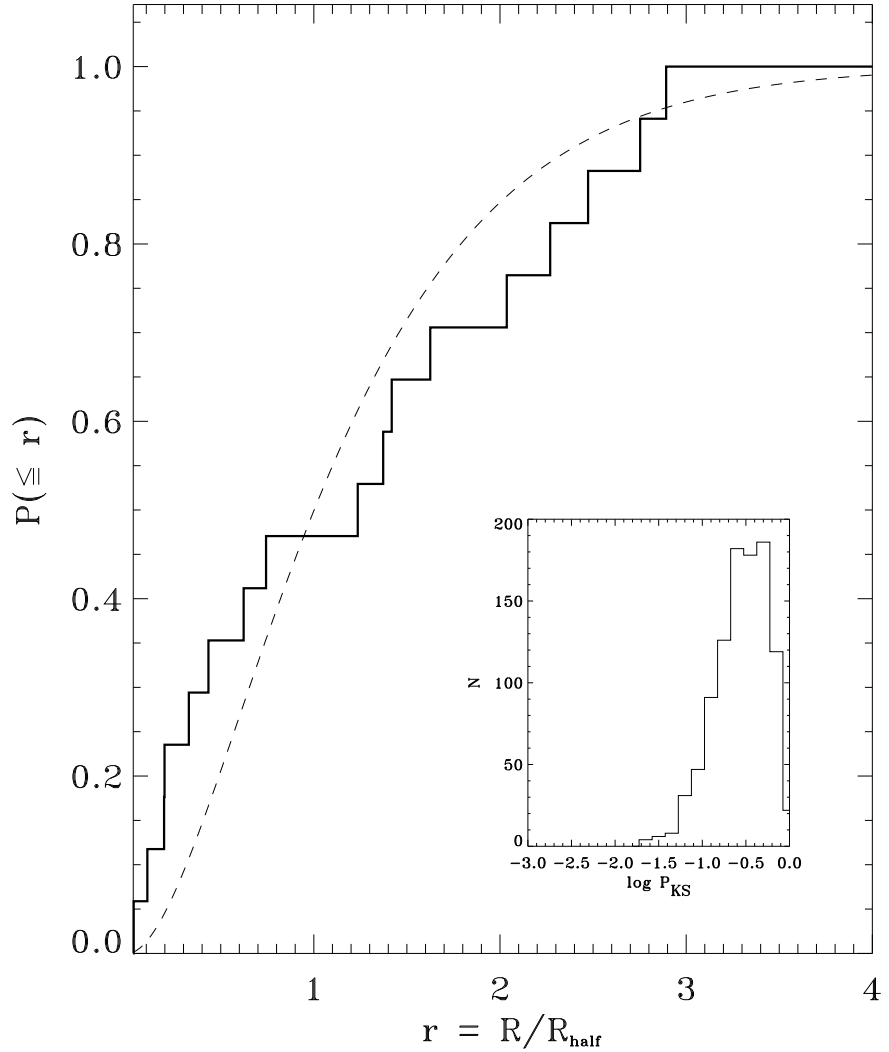


Fig. 8.— Offset distribution of GRBs compared with host galaxy star formation model. The model, an exponential disk, is shown as the smooth curve and was chosen as an approximation to the distribution of the location of collapsars and promptly bursting remnant binaries (He–He and BH–WD). The cumulative histogram is the observed data set. Inset is the distribution of KS statistics (based on the maximum deviation from the predicted and observed distribution) of 1000 synthetic data sets. Since the observed KS statistic is near the median in both cases, we are assured that errors on the measurements do not bias the results of the KS test, and therefore the KS test is robust. The observed GRB distribution provides a remarkable fit to the model considering we make few assumptions to perform the comparison.

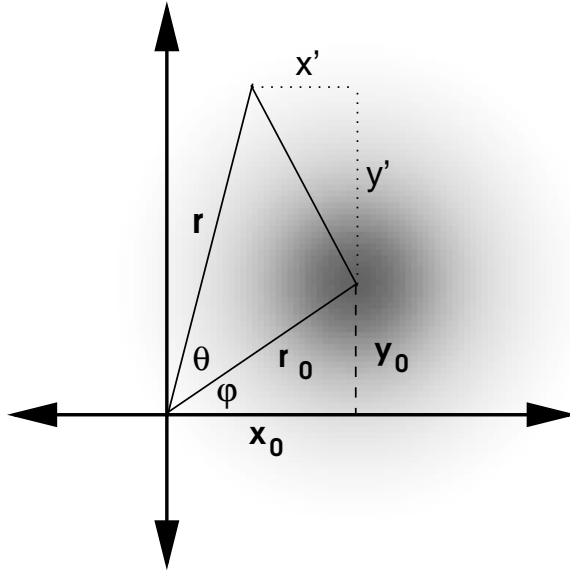


Fig. 9.— Geometry for the offset distribution probability calculation in Appendix B.

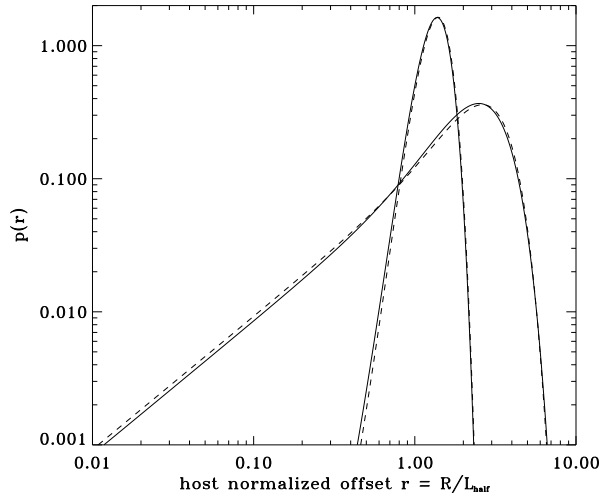


Fig. 10.— Example offset distribution functions $p(r)$. Depicted are two probability distribution curves for $(X_0, Y_0, \sigma_{X_0}, \sigma_{Y_0}, R_{\text{half}}, \sigma_{R_{\text{half}}}) = [0''.033, 0''.424, 0''.034, 0.''034, 0''.31, 0''.05]$ (GRB 970228) and $[0''.616, 0''.426, 0''.361, 0''.246, 0''.314, 0''.094]$ (GRB 981226) for the lower and upper peaked distributions, respectively. The solid line is the exact solution (eq. B2) and the dashed line is the approximate solution (eq. B3). Here, as in the text, the host-normalized offset $r = R/R_{\text{half}}$, where R is the galactocentric offset of the GRB from the host and R_{half} is the half-light radius of the host.

Table 1. GRB Host and Astrometry Observing Log

Name (1)	Teles./Instr./Filter (2)	Date (3)	α (J2000) (4)	δ (J2000) (4)	Exp. (5)	Δt (6)	Level (7)	Refs. (8)
GRB 970228...	HST/STIS/049001040	4.75 Sep 1997	05 01 46.7	+11 46 54	4600	189	self-HST	1, 2
GRB 970508...	HST/STIS/041C01DIM	2.64 Jun 1997	06 53 49.5	+79 16 20	5000	25	HST→HST	3, 4
	HST/STIS/04XB01I9Q	6.01 Aug 1997			11568	89		5
GRB 970828...	Keck/LRIS/ <i>R</i> -band	19.4 Jul 1998	18 08 34.2	+59 18 52	600	325	VLA→GB	6, 7
GRB 971214...	Keck/LRIS/ <i>I</i> -band	16.52 Dec 1997	11 56 26.0	+65 12 00	1080	1.5	GB→HST	8
	HST/STIS/04T301040	13.27 Apr 1998			11862	119		9
GRB 980326...	Keck/LRIS/ <i>R</i> -band	28.25 Mar 1998	08 36 34.3	-18 51 24	240	1.4	GB→GB	10, 11
	Keck/LRIS/ <i>R</i> -band	18.50 Dec 1998			2400	267		11
GRB 980329...	Keck/LRIS/ <i>R</i> -band	29.57 Nov 1998	07 02 38.0	+38 50 44	1800	275	VLA→GB	12, a
SN 1998bw ...	NTT/EMMI/ <i>I</i> -band	4.41 May 1998	19 35 03.3	-52 50 45	120	8.5	GB→HST	13
(GRB 980425?)	HST/STIS/065K30B1Q	11.98 Jun 2000			1185	778		14
GRB 980519...	P200/COSMIC/ <i>R</i> -band	20.48 May 1998	23 22 21.5	+77 15 43	480	1.0	GB→GB→HST	15, 16
	Keck/LRIS/ <i>R</i> -band	24.50 Aug 1998			2100	97		17
	HST/STIS/065K41IEQ	7.24 Jun 2000			8924	750		18
GRB 980613...	Keck/LRIS/ <i>R</i> -band	16.29 Jun 1998	10 17 57.6	+71 27 26	600	3.1	GB→GB	19, a
	Keck/LRIS/ <i>R</i> -band	29.62 Nov 1998			900	169		a
GRB 980703...	Keck/LRIS/ <i>R</i> -band	6.61 Jul 1998	23 59 06.7	+08 35 07	600	3.4	GB→HST	20
	HST/STIS/065K61XTQ	18.81 Jun 2000			5118	717		21
GRB 981226...	Keck/LRIS/ <i>R</i> -band	21.57 Jun 1999	23 29 37.2	-23 55 54	3360	177	VLA→GB→HST	22
	HST/STIS/065K71AXQ	3.56 Jul 2000			8265	555		23
GRB 990123...	HST/STIS/059601060	9.12 Feb 1999	15 25 30.3	+44 45 59	7200	16.7	self-HST	24
GRB 990506...	Keck/LRIS/ <i>R</i> -band	11.25 Jun 1999	11 54 50.1	-26 40 35	1560	36	VLA→GB→HST	25
	HST/STIS/065KA1UYQ	24.55 Jun 2000			7856	415		26
GRB 990510...	HST/STIS/059273LCQ	17.95 Jun 1999	13 38 07.7	-80 29 49	7440	39	HST→HST	27, 28
	HST/STIS/059276C7Q	29.45 Apr 2000			5840	355		29
GRB 990705...	NTT/SOFI/ <i>H</i> -band	5.90 Jul 1999	05 09 54.5	-72 07 53	1200	0.23	GB→GB→HST	30
	VLT/FORS1/ <i>V</i> -band	10.40 Jul 1999			1800	4.7		30
	HST/STIS/065KB1G2Q	26.06 Jul 2000			8792	386		31
GRB 990712...	HST/STIS/059262VEQ	29.50 Aug 1999	22 31 53.1	-73 24 28	8160	48	HST→HST	32, 33
	HST/STIS/059274BNQ	24.21 Apr 2000			3720	287		34
GRB 991208...	Keck/NIRSPEC/ <i>K</i> -band	16.68 Dec 1999	16 33 53.5	+46 27 21	1560	8.5	GB→GB	35, 36
	Keck/ESI/ <i>R</i> -band	4.54 Apr 2000			1260	118		37
GRB 991216...	Keck/ESI/ <i>R</i> -band	29.41 Dec 1999	05 09 31.2	+11 17 07	600	13	GB→GB→HST	38, a
	Keck/ESI/ <i>R</i> -band	4.23 Apr 2000			2600	110		a
	HST/STIS/059272GIQ	17.71 Apr 2000			9440	123		39
GRB 000301C...	HST/STIS/059277P9Q	19.49 Apr 2000	16 20 18.6	+29 26 36	8801	49	self-HST	40, 41

Table 1—Continued

Name (1)	Teles./Instr./Filter (2)	Date (3)	α (J2000) (4)	δ (J2000) (4)	Exp. (5)	Δt (6)	Level (7)	Refs. (8)
GRB 000418...	Keck/ESI/ <i>R</i> -band	28.41 Apr 2000	12 25 19.3	+20 06 11	300	10	GB→GB	42, 43
	Keck/ESI/ <i>I</i> -band	2.30 May 2000			1200	14		a
	HST/STIS/059264Y6Q	4.23 Jun 2000			2500	47		44

Note. — (2) Telescopes: HST = *Hubble Space Telescope* Keck = W. M. Keck 10 m Telescope II, Mauna Kea, Hawaii, P200 = Hale 200-inch Telescope at Palomar Observatory, Palomar Mountain, California, NTT = European Space Agency 3.5 m New Technology Telescope, Chile, VLT = Very Large Telescope UT-1 (“Antu”); Instruments: STIS (Kimble et al. 1998), ESI (Epps & Miller 1998), LRIS (Oke et al. 1995), COSMIC (Kells et al. 1998), NIRSPEC (McLean et al. 1998), SOFI (Finger et al. 1998), FORS1 (Nicklas et al. 1997); Filter: all ground-based observations are listed in standard bandpass filters while the HST/STIS images (used for astrometry) are all in Clear Mode. The last dataset of the HST visit is listed. (3) Observation dates in Universal Time (UT) corresponding to the start of the last observation in the dataset. (4) Position (α : hours, minutes, seconds and δ : degrees, arcminutes, and arcseconds) of the GRB. (5) Total exposure time in seconds. (6) Time in days since the trigger time of the GRB. (7) The comment denotes the astrometric level as in §4. (8) Reference to the first presentation of the given dataset. If two references appear on a given line then the first is a reference to the position of the GRB.

References. — a. This paper; 1. van Paradijs et al. (1997); 2. Fruchter et al. (1999); 3. Frail et al. (1997); 4. Pian et al. (1998); 5. Fruchter & Pian (1998); 6. Groot et al. (1998a); 7. Djorgovski et al. (2000); 8. Kulkarni et al. (1998); 9. Odewhan et al. (1998); 10. Groot et al. (1998b); 11. Bloom et al. (1999); 12. Taylor et al. (1998a); 13. Galama et al. (1998); 14. Holland et al. (2000a); dgk. Djorgovski et al. (1998); 17. Bloom et al. (1998); 18. Holland et al. (2000b); 19. Hjorth et al. (1998); 20. Bloom et al. (1998); 21. Bloom et al. (2000b); 22. Frail et al. (1999); 23. Hjorth et al. (2000b); 24. Bloom et al. (1999a); 25. Taylor et al. (2000); 26. Hjorth et al. (2000a); 27. Vreeswijk et al. (1999); 28. Fruchter et al. (1999b); 29. Bloom (1999); 30. Masetti et al. (2000); 31. Holland et al. (2000c); 32. Sahu et al. (2000); 33. Fruchter et al. (2000b); 34. Fruchter et al. (2000c); 35. Frail et al. (2000b); 36. Bloom et al. (2000a); 37. Diercks et al. (2000a); 38. Uglesich et al. (2000); 39. Vreeswijk et al. (2000); 40. Fynbo et al. (2000); 41. Fruchter et al. (2000a); 42. Mirabal et al. (2000); 43. Bloom et al. (2000c); 44. Metzger et al. (2000)

Table 2. Measured angular offsets and physical projections

Name	X_0 East "	Y_0 North "	R_0 "	R_0/σ_{R_0}	z	D_θ kpc/''	X_0 (proj) kpc	Y_0 (proj) kpc	R_0 (proj) kpc
GRB 970228	-0.033±0.034	-0.424±0.034	0.426±0.034	12.59	0.695	7.673	-0.251±0.259	-3.256±0.259	3.266±0.259
GRB 970508	0.011±0.011	0.001±0.012	0.011±0.011	1.004	0.835	8.201	0.090±0.090	0.008±0.098	0.091±0.090
GRB 970828	0.440±0.516	0.177±0.447	0.474±0.507	0.935	0.958	8.534	3.755±4.403	1.510±3.815	4.047±4.327
GRB 971214	0.120±0.070	-0.070±0.070	0.139±0.070	1.985	3.418	7.952	0.954±0.557	-0.557±0.557	1.105±0.557
GRB 980326	(2.570±0.150)	(0.300±0.150)	(2.587±0.150)	(17.25)	~ 1
GRB 980329	-0.303±0.371	-0.052±0.362	0.307±0.371	0.829	≤ 3.5
GRB 980425	-10.55±0.052	-6.798±0.052	12.55±0.052	241.4	0.008	0.186	-1.964±0.010	-1.265±0.010	2.337±0.010
GRB 980519	-0.050±0.130	1.100±0.100	1.101±0.100	11.01
GRB 980613	0.519±0.126	-0.827±0.144	0.976±0.135	7.232	1.096	8.796	4.565±1.108	-7.274±1.267	8.588±1.187
GRB 980703	-0.054±0.055	0.098±0.065	0.112±0.063	1.789	0.966	8.553	-0.460±0.469	0.842±0.555	0.959±0.536
GRB 981226	0.616±0.361	0.426±0.246	0.749±0.328	2.283
GRB 990123	-0.192±0.003	-0.641±0.003	0.669±0.003	223.0	1.600	9.124	-1.752±0.027	-5.849±0.027	6.105±0.027
GRB 990506	-0.246±0.432	0.166±0.513	0.297±0.459	0.647	1.310	9.030	-2.221±3.901	1.499±4.632	2.680±4.145
GRB 990510	0.064±0.009	0.015±0.012	0.066±0.009	7.304	1.619	9.124	0.584±0.082	0.137±0.109	0.600±0.082
GRB 990705	-0.805±0.075	0.145±0.075	0.818±0.075	10.91	~ 0.25
GRB 990712	-0.035±0.080	0.035±0.080	0.049±0.080	0.619	0.434	6.072	-0.213±0.486	0.213±0.486	0.301±0.486
GRB 991208	-0.052±0.065	0.043±0.061	0.067±0.063	1.071	0.706	7.720	-0.401±0.502	0.332±0.471	0.521±0.486
GRB 991216	0.211±0.029	0.290±0.034	0.359±0.032	11.21	1.020	8.664	1.828±0.251	2.513±0.295	3.107±0.277
GRB 000301C	(0.925±0.007)	(-1.918±0.007)	(2.129±0.007)	(304.2)	2.030	9.000	(8.325±0.063)	(-17.26±0.063)	(19.16±0.063)
GRB 000418	0.007±0.036	-0.035±0.041	0.036±0.041	0.871	1.118	8.829	0.062±0.318	-0.309±0.362	0.315±0.362

Note. — The observed offsets (X_0, Y_0) and associated Gaussian uncertainties include all statistical errors from the astrometric mapping and OT+host centroid measurements. The observed offset, $R_0 = \sqrt{X_0^2 + Y_0^2}$, and σ_{R_0} (constructed analogously to eq. B4) are given in col. 4. Note that $R_0 - \sigma_{R_0} \leq R \leq R_0 + \sigma_{R_0}$ is not necessarily the 68% percent confidence region of the true offset since the probability distribution is not Gaussian (see eq. B3). The term R_0/σ_{R_0} in col. 5 indicates how well the offset from the host center is determined. In general, we consider the GRB to be significantly displaced from the host center if $R_0/\sigma_{R_0} \gtrsim 5$. In col. 6, z is the measured redshift of the host galaxy and/or absorption redshift of the GRB compiled from the literature (cf. Kulkarni et al. 2000). In col. 7, D_θ is the conversion of angular displacement in arcseconds to projected physical distance.

Table 3. Host-normalized offsets

Name	R_0 ''	R_{half} (obs) ''	R_{half} (calc) ''	r_0
GRB 970228	0.426±0.034	0.31	0.308±0.092	1.373±0.247
GRB 970508	0.011±0.011	0.34	0.270±0.081	0.032±0.033
GRB 970828	0.474±0.507	...	0.292±0.088	1.625±1.805
GRB 971214	0.139±0.070	0.32	0.275±0.082	0.434±0.229
GRB 980326	(2.587±0.150)	...	(0.234±0.070)	(11.05±3.375)
GRB 980329	0.307±0.371	...	0.249±0.075	1.236±1.537
GRB 980425	12.55±0.052	18.70	...	0.671±0.003
GRB 980519	1.101±0.100	0.40	0.253±0.076	2.753±0.425
GRB 980613	0.976±0.135	...	0.338±0.101	2.892±0.955
GRB 980703	0.112±0.063	0.18	0.379±0.114	0.623±0.389
GRB 981226	0.749±0.328	0.33	0.314±0.094	2.270±1.052
GRB 990123	0.669±0.003	...	0.329±0.099	2.037±0.611
GRB 990506	0.297±0.459	0.12	0.323±0.097	2.473±3.961
GRB 990510	0.066±0.009	...	0.200±0.060	0.329±0.108
GRB 990705	0.818±0.075	1.10	0.377±0.113	0.744±0.076
GRB 990712	0.049±0.080	0.25	0.398±0.119	0.198±0.322
GRB 991208	0.067±0.063	...	0.345±0.103	0.196±0.192
GRB 991216	0.359±0.032	...	0.253±0.076	1.418±0.444
GRB 000301C	(2.129±0.007)	(0.22)	(0.329±0.099)	(9.679±2.200)
GRB 000418	0.036±0.041	...	0.338±0.101	0.106±0.126

Note. — $R_0 = \sqrt{X_0^2 + Y_0^2}$ is the observed offset from col. 4 of Table 2. The half-light radius R_{half} is observed from HST imaging (col. 3) or calculated using the magnitude-radius empirical relationship (col. 4; see text). The uncertainty is taken as 0''.05 (1- σ) for HST imaging (col. 3) or 30% of the calculated radius (col. 4). The host-normalized offset $r_0 = R_0/R_{\text{half}}$ given in col. 5 is derived from (if possible) the observed half-light radius or the calculated half-light radius (otherwise). The error on r_0 is σ_r from eq. B4. Note that $r_0 - \sigma_r \leq r \leq r_0 + \sigma_r$ is not necessarily the 68% percent confidence region of the true offset since the probability distribution is not Gaussian.